Divergent responses to SARS-CoV-2 infection in bronchial epithelium with pre-existing respiratory diseases

Justine Oliva, Manon Ruffin, Claire Calmel, Aurélien Gibeaud, Andrés Pizzorno, Clémence Gaudin, Solenne Chardonnet, Viviane de Almeida Bastos, Manuel Rosa-Calatrava, Antoine Soulé, et al.

Journal Pre-proof

Divergent responses to SARS-CoV-2 infection in bronchial epithelium with pre-existing respiratory diseases

Justine Oliva, Manon Ruffin, Claire Calmel, Aurélien Gibeaud, Andrés Pizzorno, Clémence Gaudin, Solenne Chardonnet, Viviane de Almeida Bastos, Manuel Rosa-Calatrava, Antoine Soulé, Amin Emad, Simon Rousseau, Harriet Corvol, Olivier Terrier, Loïc Guillot

PII: S2589-0042(25)00259-7

DOI: https://doi.org/10.1016/j.isci.2025.111999

Reference: ISCI 111999

To appear in: *ISCIENCE*

Received Date: 8 October 2024

Revised Date: 4 December 2024

Accepted Date: 7 February 2025

Please cite this article as: Oliva, J., Ruffin, M., Calmel, C., Gibeaud, A., Pizzorno, A., Gaudin, C., Chardonnet, S., de Almeida Bastos, V., Rosa-Calatrava, M., Soulé, A., Emad, A., Rousseau, S., Corvol, H., Terrier, O., Guillot, L., Divergent responses to SARS-CoV-2 infection in bronchial epithelium with pre-existing respiratory diseases, *ISCIENCE* (2025), doi: https://doi.org/10.1016/j.isci.2025.111999.

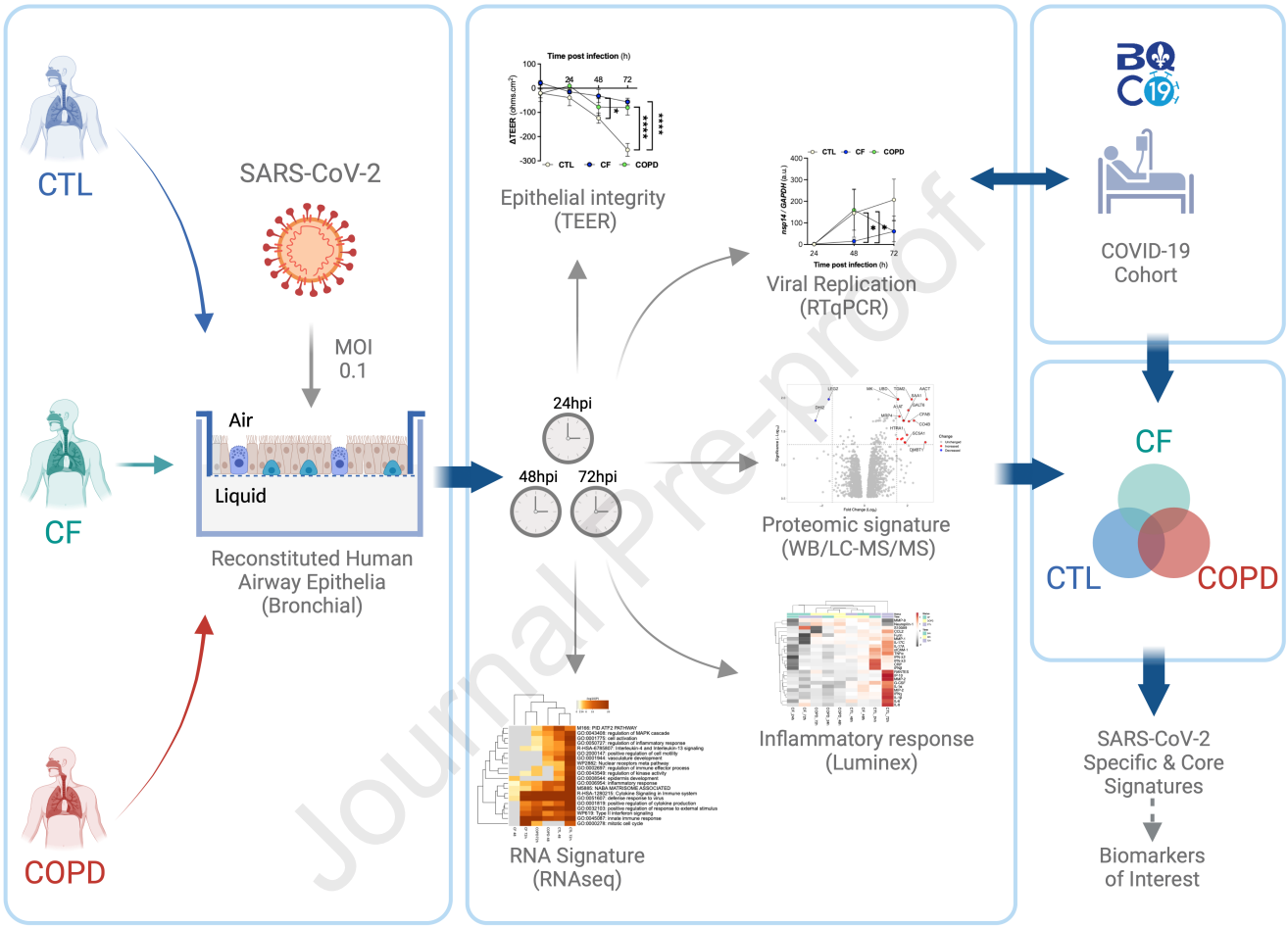

Divergent responses to SARS-CoV-2 infection in bronchial epithelium with pre-existing respiratory diseases

Justine Oliva[1#], Manon Ruffin[2#], Claire Calmel[2], Aurélien Gibeaud[1], Andrés Pizzorno[1], Clémence Gaudin, Solenne Chardonnet[3], Viviane de Almeida Bastos[3], Manuel Rosa-Calatrava[1], Antoine Soulé[4], Amin Emad[5], Simon Rousseau[6], Harriet Corvol[2,7], Olivier Terrier[1‡*] and Loïc Guillot[2‡**]

[1]CIRI, Centre International de Recherche en Infectiologie, Team VirPath, Université de Lyon, INSERM U1111, Université Claude Bernard Lyon 1, CNRS, UMR5308, ENS de Lyon, 69007 Lyon, France

[2]Sorbonne Université, INSERM, Centre de Recherche Saint-Antoine (CRSA), 75012, Paris, France

[3]Sorbonne Université, INSERM, UMS PASS, Plateforme Post-génomique de la Pitié-Salpêtrière (P3S), 75013 Paris, France

[4]Department of Electrical and Computer Engineering, McGill University, Montréal, QC, Canada

[5]Mila, Québec AI Institute, Montréal, QC, Canada

[6]The Meakins-Christie Laboratories at the Research Institute of the McGill University Health Centre Research Institute, & Department of Medicine, Faculty of Medicine, McGill University, Montréal, QC, Canada

[7]Pneumologie Pédiatrique, APHP, Hôpital Trousseau, 75012, Paris, France

[#] These authors contributed equally to this work as co-first authors.

[‡]These authors contributed equally to this work as co-last authors.

Lead contact: Loïc Guillot (loic.guillot@inserm.fr)

Corresponding authors:

[*]O Terrier, CIRI, Campus de La Buire, Bat B, 2eme Étage, 11 Rue G. Paradin 69372 Lyon, France

Tel: +33(0)478778704

E-mail: olivier.terrier@univ-lyon1.fr

**L Guillot, Inserm UMR S 938, CRSA, Bât. Kourilsky, 34 Rue Crozatier, 75012 Paris, France ;

Tel: +33 149 284 682

E-mail: loic.guillot@inserm.fr

Summary

Pre-existing respiratory diseases may influence coronavirus disease (COVID-19) susceptibility and severity. However, the molecular mechanisms underlying the airway epithelial response to severe acute respiratory syndrome coronavirus 2 (SARS-CoV-2) infection severity in patients with chronic respiratory diseases remain unelucidated. Using an *in vitro* model of differentiated primary bronchial epithelial cells, we aimed to investigate the molecular mechanisms of SARS-CoV-2 infection in pre-existing cystic fibrosis (CF) and chronic obstructive pulmonary disease (COPD). Our study revealed reduced susceptibility of CF and COPD airway epithelia to SARS-CoV-2, relative to that in healthy controls. Mechanistically, reduced transmembrane serine protease 2 (TMPRSS2) activity potentially contributed to this resistance of CF epithelium. Upregulated complement and inflammatory pathways in CF and COPD epithelia potentially primed the antiviral state prior to infection. Analysis of a COVID-19 patient cohort validated our findings, correlating specific inflammatory markers (IP-10, SERPINA1, and CFB) with COVID-19 severity. This study elucidates SARS-CoV-2 pathogenesis and identifies potential biomarkers for clinical monitoring.

Keywords: Cystic Fibrosis, COPD, COVID-19, SARS-CoV-2, Respiratory epithelium, chronic obstructive pulmonary diseases

Introduction

The coronavirus disease (COVID-19) pandemic has underscored individual variations in the susceptibility and severity of severe acute respiratory syndrome coronavirus 2 (SARS-CoV-2) infections. The major risk factors for severe illness include age, immunocompromised status, and underlying comorbidities. Hypertension, diabetes and cardiovascular disease confer a high risk of severe COVID-19[1].

At the onset of the pandemic, individuals with pre-existing impaired lung function due to chronic respiratory diseases such as cystic fibrosis (CF), asthma, or chronic obstructive pulmonary disease (COPD) were considered potentially more vulnerable. Follow-up clinical studies have revealed varying susceptibility levels and risks of severe COVID-19 among these patient populations[2]. People with CF (pwCF), particularly those who have undergone lung transplantation, are at increased risk of severe disease and mortality following SARS-CoV-2 infection[3,4]. Numerous cohort studies and meta-analyses have demonstrated an increased likelihood of severe hospitalisation and mortality among patients with COPD[5-7] but not necessarily among those with asthma[7,8]. However, conflicting results have emerged because asthma is treated as a single condition without differentiation based on its type and severity.

Despite follow-up clinical studies, limited research has been conducted to understand and model whether patients with preexisting conditions are more susceptible to severe COVID-19. To date, research has primarily focused on the virus entry receptors, angiotensin-converting enzyme 2 (ACE2), and transmembrane serine protease (TMPRSS2), which are overexpressed in smokers and patients with COPD, but not in those with asthma[2]. However, ACE2 expression varies and depends on the type of asthma, with low expressions associated with type 2 asthma and atopic inflammation[2]. At the cellular level, SARS-CoV-2 targets epithelial cells of the respiratory tract, starting from the nasal cells of the upper respiratory tract and progressing to the alveolar epithelial cells. In addition to their importance in the infection process, these epithelial cells play crucial roles in both innate immunity and the initiation of an adaptive immune response[2], as well as in their interactions with immune cells to condition disease severity[9].

However, the molecular mechanisms underlying the response of the airway epithelium to SARS-CoV-2 infection in patients with chronic respiratory diseases remain poorly understood. In this study, we aimed to model SARS-CoV-2 infection in the context of pre-existing respiratory conditions, specifically CF and COPD. Our objective was to investigate the influence of specific characteristics of the epithelial response on the outcome of SARS-CoV-2 infection in these pathological conditions. We used an *in vitro* SARS-CoV-2 infection model involving differentiated primary bronchial epithelial cells cultured at an air-liquid interface (ALI)[10]. These cells were derived from healthy individuals and patients with CF or COPD. We used an integrated strategy combining virological, physiological, transcriptomic, and proteomic approaches to highlight the common or characteristic signatures of SARS-CoV-2 infection in these different contexts. We further compared the identified signatures with clinical data through a retrospective analysis of a large cohort of patients with COVID-19.

Results

Differential impact of SARS-CoV-2 on the integrity of the control, CF, and COPD epithelia

We aimed to assess the differential impact of SARS-CoV-2 on the response of human airway epithelial (HAE) cell models relative to those in the control (CTL), cystic fibrosis (CF), and chronic obstructive pulmonary disease (COPD) epithelia (**Fig 1. A**) Initially, the transepithelial electrical resistance (TEER) was determined, to evaluate epithelial integrity (**Fig. 1B-D**). The baseline TEER values before viral infection were lower in the CF and COPD groups than those in the CTL group, reflecting inherent physiological differences in each model (**Fig. 1B-D**). In all groups, whether in infected or uninfected conditions, we observe an increase in TEER at 24 h, which returns to the initial state at 48 h (**Fig. 1B-D**). Following SARS-CoV-2 infection, the CTL group exhibited a more substantial reduction in TEER (68% decrease at 72 [hours post-infection (hpi); $p<0.0001$, **Fig. 1B**] than that in the CF (35% decrease; $p<0.05$, **Fig. 1C**) and COPD (38% decrease; **Fig. 1D**) groups. Thus, CF and COPD epithelia may be more resistant to SARS-CoV-2 infection. To compare the impact of SARS-CoV-2 on epithelial integrity across groups, we calculated the TEER change (ΔTEER) between infected and mock-infected conditions at each time point. The findings revealed a more substantial impairment of airway epithelial integrity after SARS-CoV-2 infection in the CTL group than those in the CF and COPD groups (**Fig. 1E**). No significant differences in viral quantification were observed on the apical surface of the epithelium among the three groups, with levels reaching a plateau at 24 hours post-infection (**Fig. 1F**). However, quantification of intracellular viral genome expression (*nsp14* mRNA levels) with time showed lower SARS-CoV-2 replication in the CF group, with only a slight increase at 72 hpi (**Fig. 1G**). In contrast, the CTL and COPD groups exhibited similar trends between 24 and 48 hpi, with a notable increase in *nsp14* mRNA expression. Interestingly, SARS-CoV-2 replication sharply declined in the COPD group at 72 hpi, returning to a level similar to that in the CF group, whereas *nsp14* mRNA expression slightly increased in the CTL group. Finally, we observed that SARS-CoV-2 infection led to a loss of ZO-1 expression in HAE CTL cells (**Fig. 1H**). Overall, our findings suggest more pronounced SARS-CoV-2 replication in the CTL than that in the CF and COPD HAE models, which correlates with a greater impact on epithelial integrity.

SARS-CoV-2 induces an epithelial type-specific transcriptomic responses over time

The transcriptomic response to SARS-CoV-2 in the CTL group was initiated at 48 h, revealing 135 differentially expressed genes (DEGs) relative to those in the mock-infected group, 132 of which were overexpressed. This response was further amplified at 72 h, with 1275 DEGs, of which 970 were overexpressed (see **Fig. 2A** and **Table S1**). Analysis of the associated enriched biological pathways notably highlighted the "innate immune response" (GO:0045087) pathway (**Fig. 2B**). At 72 hpi, numerous genes of the interferon (IFN) family, including *IFNB1* (encoding IFN-β), *IFNL1* (encoding IFN-λ1 or IL-29), *IFNL2* (encoding IFN-λ2 or IL28A), *IFNL3* (encoding IFN-λ3 or IL28B), and *CXCL10* (encoding interferon gamma-inducible protein 10 kDa (IP-10)), were among the top 15 most-induced DEGs (**Fig. 2C**). At the protein level, this inflammatory response manifests through the induction of IP-10 (**Fig. 2D**), Granulocyte colony-stimulating factor (G-CSF; **Fig. 2E**), RANTES (**Fig. 2F**), IL-1β (**Fig. 2G**), IFN-λ3 (or IL-28B; **Fig. 2H**), tumour necrosis factor-α (TNF-α; **Fig. 2I**), IL-17A (**Fig. 2J**), IFN-γ (**Fig. 2K**), and IL-8 (**Fig. 2L**) at 72 hpi. However, the infection did not affect the production of the other tested mediators (**Fig. S1** and **Fig. S2**).

In the CF group, the transcriptomic response to SARS-CoV-2 initiated at 48 hpi, involving 20 DEGs, of which 19 were overexpressed. At 72 h, 135 DEGs including 128 overexpressed transcripts were identified (**Fig. 3A** and **Table S2**). The analysis of associated enriched biological pathways notably revealed the activation of "antiviral mechanism by IFN-stimulating genes" (R-HSA-1169410) and "defence response to virus" (GO:0051607) pathways (**Fig. 3B**). At 72 hpi, *CXCL10*, *CXCL11*, *C11orf96*, ZBP1, and *IFIT2* were among the top 15 most-induced DEGs (**Fig. 3C**). Among the mediators measured at the protein level, only MMP-9 production was affected and downregulated at 24 hpi (**Fig. 3D**, **Fig. S1** and **Fig. S2**).

Similar to the CTL and CF groups, the response to the virus in the COPD group was detected only at the transcriptomic level from 48 h. It was characterised by 79 DEGs (including 78 overexpressed genes) at 72 hpi (**Fig. 3E** and **Table S3**). Enriched biological pathways included "defence response to virus" (GO:0051607) and "SARS-CoV-2 innate immunity evasion cell-specific immune response pathways" (WP5039) (**Fig. 3F**). At 72 hpi, *IFNB1, IFNL1, IFNL2, IFNL3,* and *CXCL11* were among the top 15

most-induced genes (**Fig. 3G**). At the protein level, only IP-10 production was affected and was upregulated at 72 hpi (**Fig. 3H** and **Fig. S1** and **Fig. S2**).

SARS-CoV-2 induces a stronger inflammatory response in epithelium from healthy donors than from CF and COPD patients

A comparative analysis was conducted to investigate the reduced susceptibility of CF and COPD epithelia to SARS-CoV-2 infection, relative to the CTL epithelia. Overall, the effect of SARS-CoV-2 infection on each group (CTL, CF, and COPD) revealed an increased number of transcripts from 48 h onwards. However, this increase was notably greater at 72 h in the CTL group than that in the other two pathological groups (**Fig. 4A**). The following three DEGs were common to all three groups at both 48 and 72 hpi : *SOCS1*, *ZBP1*, and *CXCL10* (**Fig. 4B and Fig. S3**). Functional enrichment analysis at 48 and 72 hpi unveiled two major common pathways, "cytokine signalling in the immune system" (R-HAS-1280215) and "defence response to virus" (GO:0051607) (**Fig. 4C**). In the CF group, this response was mainly detected at 72 hpi, whereas in the CTL and COPD groups, it was observed as early as 48 hpi, with the CTL group exhibiting the strongest activation (**Fig. 4C**). Comparative analysis at 72 hpi, the time when the number of induced genes is maximal (**Fig. 4A**), revealed a distinct response, mainly between the CF and CTL groups, with 193 specific DEGs (**Fig. 4D** and **Table S4**). Biological pathway enrichment analysis notably supported the involvement of the “complement and coagulation cascade” and “TGF-β signalling pathway” in the specific response of the CF group (**Fig. 4E**). No significant enrichment was observed in the COPD-specific response at 72 hpi. Comparative analysis at 24 hpi revealed a distinct response, primarily between the CF and CTL groups, with 159 specific DEGs (**Fig S4A** and **Table S4**). Biological pathway enrichment analysis (only feasible in the CF group with sufficient DEGs) highlighted the involvement of “NF-κB, TNF-α, and IL-17 signalling” pathways. Few DEGs were identified between the COPD and CTL or the CF and COPD groups at 24 hpi. At 48 hpi (**Fig S4B** and **Table S4**) and 72 hpi (**Fig. 4C** and **Table S4**), a slight increase of the number of DEGs was observed between the CF and CTL groups (165 and 193 specific DEGs, respectively), as well as between the COPD and CTL groups (25 and 26 specific DEGs, respectively). Finally, enrichment

analysis at 48 h supported the involvement of "NF-κB and IL-17 signalling pathway" and "TNF and IL-17 signalling pathways" in the specific responses of the CF and COPD groups, respectively (**Fig S4B**). A comparative analysis of the infection effects between groups at different infection times (intersection: (CTL non-infected (ni) vs. infected (pi)) vs. (disease group ni vs. pi)) was conducted. The only difference in transcript expression was observed at 72 h between the CF and CTL groups (126 genes), as well as between the COPD and CTL groups (45 genes) (**Fig S5** and **Table S5**). Apart from the 28 common genes, 17 genes were specific to the COPD HAE response, and 28 genes were specific to the CF HAE response. Enrichment analysis revealed that the "TNF signalling pathway" was involved in, both, the CF and COPD groups. In contrast, no DEGs were observed between the CF and COPD groups. The inflammatory response was further investigated by comparing the secretion of various cytokines among the three groups. Overall, a stronger inflammatory response was observed in the CTL group at 72 h than in the other pathological groups, as shown by the heat map (**Fig. 5A** and **Fig. S6A-K**), with in particular a strong increase in the level of IP-10 expression compared to those of the CF and COPD groups **(Fig. 5B**). At 24 h, a significant increase in G-CSF expression levels was observed in the CTL HAE group compared to those in the CF and COPD groups (**Fig. S6A**). Additionally, a significant increase in IL-17A levels was observed in the CTL group compared to that in the CF group (**Fig. S6A**). No significant differences were observed at 48 h; however, higher expression levels of G-CSF, RANTES, MMP-1, S100A9, CCL-2, MIP-2, Furin, IFN-γ, IL-1β, and TNF-α (**Fig. S6A-K**) were observed in the CTL group at 72 h compared to those in the CF and COPD groups. In contrast, no variations in IFN-λ2, IFN-β, IL-8, IL-6, IL-1α, IL-17C, CRP, MMP-9, MMP2, and neuropilin secretion levels were observed between the disease groups (**data not shown**).

Interestingly, increased soluble intercellular adhesion molecule 1 (sICAM-1) levels were observed at 72 h in the CTL group compared to those in the CF and COPD groups (**Fig. 5C**). Despite these data suggesting induction at this time point, we did not observe a significant difference in sICAM-1 secretion between non-infected and infected CTL HAE (**Fig. 5D**), contrary to the RNA-sequencing (RNA-seq) results (**Fig. 5E**). These data suggest a delay between the increase in mRNA expression and secretion of soluble ICAM-1. Consistently, we compared the induction of intracellular ICAM-1 between non-

infected and infected conditions at 72 hpi, revealing a significant induction of intracellular ICAM-1 only in the CTL group (**Fig. 5F**).

CF and COPD epithelial cells possess specific characteristics which protect them from SARS-CoV-2 infection

We aimed to rationalize the difference in antiviral response between the pathological groups. We hypothesised that although epithelial cells are isolated from the organ and cultivated *in vitro*, they retain the intrinsic properties which enable them to generate a specific innate immune response. We analysed the response in the initial state (non-infected at 24 h) of each group using both transcriptomic and proteomic approaches (**Fig. 6**). CF cells displayed a very distinct transcriptomic signature compared to CTL, with 350 DEGs. In comparison, only 46 DEGs were observed between COPD and CTL cells (**Fig. 6A** and **Table S6**). Finally, only nine specific DEGs were observed between CF and COPD cells (**Fig. 6A** and **Table S6**). Pathway enrichment analysis highlighted a strong association with the "inflammatory response" (GO:0006954) processes and "complement and coagulation cascades" (hsa04610) in the CF and COPD group (**Fig. 6B**). Interestingly, IL-6 and MUC5B/MUC5AC (**Table S6)** are among the genes most highly expressed in COPD and CF cells respectively, compared to CTL cells.

In addition, protein expression analysis revealed significant differences between the CTL and CF groups (**Fig. 6C** and **Table S7**). The 15 most differentially expressed proteins (fold change) included AACT (Alpha-1-antichymotrypsin or SERPINA3), DMBT1 (Deleted in malignant brain tumours 1 protein), CO4B (Complement C4-B), TGM2 (Protein-glutamine gamma-glutamyltransferase 2), CFAB (Complement factor B), SAA1 (Serum amyloid A-1 protein), HTRA1 (Serine protease HTRA1), SLC5A1 (Sodium/glucose cotransporter 1), RARRES (Retinoic acid receptor responder protein 1), GALT6 (Polypeptide N-acetylglucosaminyltransferase 6), A1AT (Alpha-1-antitrypsin), MIA (Melanoma-derived growth regulatory protein), CO3 (Complement C3), ABCC4 (ATP-binding cassette sub-family C member 4), UBD (Ubiquitin D), and MK (Midkine). Enrichment analysis of the 86 differentially expressed proteins (**Table S7**) notably identified 11 significantly enriched Gene Ontology (GO) terms, including “complement activation” (GO:0006956) and “regulation of peptidase activity” (GO:0052547) (**Fig. 6C**). Protein interaction network analysis revealed four clusters with one major

cluster containing 34 proteins (**Fig. 6D**). Interestingly, we also identified several proteins involved in the complement pathway. These expression profiles obtained at 24 h using proteomics and transcriptomics suggested re-evaluation of the RNA-seq data under infection conditions over time for the target genes *C3*, *CFB*, *C4B*, *C4A*, *SERPINA1*, and *SERPINA3*. Consistent with the proteomic data, the overexpressions of *C3*, *CFB*, *C4B*, *C4A*, *SERPINA1*, and *SERPINA3* were observed in CF cells at baseline (**Fig. 6E**). However, this increase is not observed in airway 16HBE14o- CF cells with different variants compared with wild-type 16HBE14o-isogenic cells (**Fig. S6I**). Finally, SARS-COV-2 induced *C4B* and *C4A* expressions in the CTL and COPD groups at 72 hpi, whereas *C3*, *CFB*, *SERPINA1*, and *SERPINA3* expressions increased only in the CTL group at 72 hpi.

We aimed to elucidate the molecular mechanisms that protect CF and COPD epithelial cells against SARS-CoV-2 infection. This could be potentially attributed to relatively lower expressions of viral receptors (ACE2 and TMPRSS2). Similar ACE2 mRNA and protein expression levels were observed in all three groups of non-infected cells at 24 h (**Fig. 6F**). Comparative *TMPRSS2* RNA expression at 24 h showed a significant reduction in the CF group (**Fig. 6F**). However, corresponding differences at the protein level were not observed using western blotting (**Fig. 6G**) or proteomic analysis (**Table S7**). Furthermore, we observed a significant 1.5-fold decrease in TMPRSS2 activity at the apical side of the CF epithelium relative to that in the CTL and COPD group, which was equivalent to that obtained with serine protease inhibitor treatment, such as mesylate camostat (**Fig. 6H**). Thus, the relative protection of CF epithelia against SARS-CoV-2 is not linked to quantitative but to functional variations in TMPRSS2. In conclusion, our analyses reveal that the initial state of bronchial epithelial cells in CF and COPD patients differs significantly from that of healthy donor cells. The pro-inflammatory condition of these cells, along with specific characteristics like the overexpression of A1AT and the reduced expression of TMPRSS2 observed in CF cells, may impact their response to SARS-CoV-2 infection.

IP-10, SERPINA1 and CFB are associated with COVID-19 infection and severity

Transcriptomic and proteomic analyses performed in HAE revealed elevated IP-10 levels in SARS-CoV-2-infected CTL, CF, and COPD epithelia. Similarly, but restricted to the CTL group, sICAM-1,

SERPINA1, SERPINA3, C3, C4, and CFB were induced by SARS-CoV-2 infection. Thus, these mediators may serve as potential clinical markers of infection and disease severity.

To validate this hypothesis, we analysed the secretion levels of these mediators in patients from the COVID-19 Quebec Biobank (BQC19, www.quebeccovidbiobank.ca) using a multiplex SOMAmer affinity array (Somalogic)[11]. The expression levels of IP-10, SERPINA1, C4, and CFB were significantly higher in the COVID-19-positive group than in the COVID-19-negative group. Conversely, sICAM-1, SERPINA3, and C3 levels were significantly lower in the COVID-19-positive group (**Fig. 7A**). Considering infection severity, we determined that IP-10, SERPINA1, and CFB levels were significantly elevated in patients with severe COVID-19 compared to those with moderate COVID-19, whereas C3 levels were reduced in the severe group. Thus, IP-10, SERPINA1, and CFB are markers of both SARS-CoV-2 infection and COVID-19 severity (**Fig. 7B**). In-line with this, further specific analysis of patients with COPD showed a significant increase in IP-10 levels in COVID-19-positive patients with COPD, compared to those without COVID-19 (**Fig. 7C**). However, a similar analysis could not be performed in patients with CF due to the limited number of cases.

Discussion

At the beginning of the COVID-19 pandemic, patients with pre-existing respiratory pathologies were expected to be at a higher risk of developing severe illnesses. Apart from clinical studies, limited experimental studies have investigated if these patients are more vulnerable to SARS-CoV-2 infection and elucidated the underlying molecular mechanisms. In this study, we investigated and compared the response of bronchial epithelial cells from healthy donors and patients with pre-existing respiratory pathologies, such as CF and COPD, to SARS-CoV-2 infection. We further determined whether the experimental models were consistent with the clinical data reported for this vulnerable population.

We used a physiologically relevant *in vitro* model of reconstituted epithelium derived from cells differentiated at the air-liquid interface from healthy lung tissue, a model previously well-characterized by our team and others in the context of SARS-CoV-2 infection[10,12]. Additionally, we included epithelia derived from pwCF and patients with COPD. Despite the inherent limitations of an *in vitro* model, these epithelia preserve key disease-specific characteristics. For instance, the CF model exhibits impaired CFTR chloride channel function[13]. Reconstituted epithelium models derived from COPD patients retain key disease-associated features, even over the long term[14].

Using this model, we observed that bronchial HAE from patients with pre-existing respiratory pathologies (CF or COPD) displayed a distinct response to infection relative to that from healthy donors. Interestingly, this response was characterised by preservation of epithelial integrity, low SARS-CoV-2 infectivity, and low antiviral and inflammatory responses. Thus, we hypothesised that individuals without excessive inflammatory responses could not develop severe COVID-19.

Based on the findings of our previous study[10], we observed that the infection of healthy donor epithelium by SARS-CoV-2 induced a loss of epithelial integrity, characterised by a decrease of TEER and the disruption of ZO-1 cell junction protein as previously shown[12,15]. This was associated with an inflammatory response characterised by IFN pathway activation, as observed using both transcriptomic and proteomic data. Interestingly, CXCL-10 (IP-10) was strongly induced at 72 hpi, as evidenced by both mRNA expression and protein secretion. Consistently, this strong CXCL-10 induction was similarly observed in another study using primary tracheobronchial and alveolar cells cultured at the air-liquid interface[16]. CXCL-10 is a well-known IFN-inducible chemokine with pleiotropic roles[17]; its levels

are increased in patients with COVID-19[18]. This cytokine is also a known nasopharyngeal biomarker of viral respiratory infection[19,20] and a systemic marker of COVID-19 severity[21]. Our experimental results are in-line with these numerous clinical studies and also correlate with our cohort analysis, wherein CXCL-10 correlated at the systemic level with SARS-CoV-2 infection and severity in the BQC19 cohort. *CXCL-10* mRNA levels, but not protein levels, were also increased 72 hpi in the CF epithelium, compared to that in healthy controls. This difference could be explained by the timing of infection, wherein a longer duration of SARS-CoV-2 infection in CF cells may be required to determine its impact on CXCL-10 protein secretion. Unfortunately, we were unable to analyse CXCL-10 secretion in pwCF from the BQC19 cohort, since data were not recorded. Interestingly, a case study reported lower CXCL-10 expression in a pwCF infected with SARS-CoV-2 than that in a pwCF without SARS-CoV-2 infection[22]. Although our experimental results corroborate these findings, it is difficult to establish an association between CXCL-10 levels and the severity of pwCF in our study, as no pwCF with COVID-19 was included in the BQC19 cohort. Similarly, CXCL-10 mRNA and protein levels were induced in the COPD epithelium. In the BQC19 cohort, we also observed an enrichment of this cytokine in patients with COPD positive for COVID-19 compared to that in patients with COPD but without COVID-19.

In the CF epithelium, viral replication was reduced and did not severely damage epithelial integrity. Our data strongly correlate with the findings of previous studies using CF cells, such as cell lines (CFBE41o-ΔF, 16HBE CFTR KO) or differentiated primary bronchial epithelial cells at the ALI[23,24]. Correspondingly, there were no differences in ACE2 expression between control and CFTR-deficient cells[23,24], suggesting that reduced SARS-CoV-2 infection is not caused by a lower viral entry. However, these results contradict those of a recent study by Bezzerri et al., which shows that ACE2 mRNA and protein expression are reduced in CF epithelium compared to that in healthy primary nasal or bronchial epithelium. They suggested that this phenomenon could explain the reduced SARS-CoV-2 replication in CF cells[25]. They also performed a similar analysis with Calu-3 CFTR-KO (SH3 cells) cells, as well as isogenic cells of the 16HBE14o-line with W1282X or G542X nonsense mutations, which supported this hypothesis. However, they also demonstrated identical ACE2 expression in CFBE41o- and CFBE41o-/F508del cells[25]. Furthermore, ACE2 expression is not modulated by CFTR inhibition[25]. Therefore, it is difficult to rule out the impact of ACE2 expression on SARS-CoV-2 infectivity in

patients with CF. In our study, western blotting or mass spectrometry did not reveal differences in ACE2 protein expression in bronchial HAE with the F508del variant, suggesting that the ACE2 expression levels in CF cells may depend on CFTR expression levels related to the type of CFTR variant (missense (e.g. F508del) vs. nonsense (e.g. G542X)). However, we cannot exclude the possibility of other inter-individual variabilities, such as sex, in ACE2 expression between donors, rather than a specific effect linked to CFTR. This hypothesis could explain the discrepant results between our study and that of Berrezzi et al[25]. Categorically, ACE2 is localized on the X chromosome and belongs to a subgroup of X chromosome genes showing higher expression in male lungs[26]. Hence, in the study by Berrezzi et al., the use of healthy male donors and female pwCF may introduce a bias in interpreting the observed difference in ACE2 expression [25].

TMPRSS2 is a critical protein involved in SARS-CoV-2 infection. It cleaves the spike protein, allowing viral entry and replication. In our experimental model, TMPRSS2 was similarly expressed in the CF and healthy epithelium. This result is consistent with a single-cell transcriptomic study involving 19 healthy donors and 19 pwCFs (both fresh airway tissue and differentiated cells at ALI), demonstrating similar ACE2 and TMPRSS2 expressions[27]. Surprisingly, we observed reduced TMPRSS2 activity in the CF epithelium compared to that in the healthy and COPD epithelium. To our knowledge, this is the first demonstration that this mechanism might be responsible for reduced SARS-CoV-2 infectivity in the CF respiratory epithelium. Interestingly, proteomic analysis of uninfected epithelia reveals a distinct regulation of peptidase activity in CF cells, highlighted by an overexpression of A1AT. This overexpression may play a role in the inhibition of TMPRSS2 activity observed in CF cells. Indeeed, A1AT has been shown to inhibit TMPRSS2 protease activity and reduce SARS-CoV-2 infection in primary human airway cells[28].

In this study, we focused on deciphering the cause of different antiviral responses between CF and COPD epithelia. Transcriptomic and proteomic analysis of the initial (non-infected) state revealed that CF and COPD bronchial HAE are already involved in the response to infection. Interestingly, proteins associated with complement pathways, such as C3 and CFB, are overexpressed intracellularly in CF epithelial cells. Interestingly, confirming this already inflammatory basal state of the CF epithelium, we also observed that MUC5B and MUC5AC transcripts are overexpressed in CF cells. MUC5B and

MUC5AC proteins are known to be increased in the sputum of pwCF[29]. Some complement and inflammatory proteins including IL-6 are also upregulated in the COPD epithelium, but only at the genomic level. The overexpression findings in our experimental model correlated with those of another study, wherein C3 was overexpressed at the intracellular level in the epithelium of pwCF[30]. Moreover, C3 is overexpressed in COPD lung tissues[30]. Kulkarni et al. suggested that the intracellular C3 protein protects airway epithelial cells from stress-associated cell death[30]. Complement hyperactivation is also a well-documented clinical feature of COVID-19[31]. However, the role of intracellular complement in the cellular response to SARS-CoV-2 infection remains unclear. While the role of complement proteins in regulating inflammatory and immune responses is well-known, their intracellular role is emerging but remains poorly understood[32]. A mechanistic study has shown that C3 is capable of binding to viruses (e.g. adenovirus) and promoting their degradation, thus preventing their replication[33]. Similar to C3, CFB plays a major role in pulmonary epithelial cell survival under stress by attenuating programmed cell death[34]. Consistent with previous findings[35], we observed no overexpression of C3 or CFB in wild-type 16HBE14o cells compared to isogenic 16HBE14o CF cells carrying various CFTR variants, suggesting that CFB and possibly C3 overexpression are unrelated to the CFTR defect. The most likely hypothesis is that this increase is linked to a history of CF, particularly the chronic colonisation of the respiratory tract of pwCF by various pathogens. Notably, *Pseudomonas aeruginosa* infection of bronchial epithelial cells increases C3 and CFB expressions[34].

Epithelial cells from COPD or CF donors infected with SARS-CoV-2 showed no or delayed decrease in integrity. The viral load in COPD cells was detectable at 48 h and in quantities similar to those of healthy epithelial cells, but decreased significantly at 72 h, reaching the level of CF epithelial cells. We did not observe any differences in viral replication in the apical medium between the different groups. While other studies have demonstrated differences in viral replication between cells from CF and non-CF donors (albeit with other respiratory pathologies and specific SARS-CoV-2 variants) using a higher MOI (MOI=1)[24], it is possible that the MOI employed in our model is excessively high. This represents a potential limitation of our study. A similar transcriptomic signature was observed between COPD and CF epithelia in our study, suggesting a common cellular response. The response of bronchial epithelial cells in patients with COPD has been documented, particularly in a study using a single-cell RNAseq

approach[36]. In this study, infected epithelial cells from healthy donors expressed lower CXCL-10 levels than those in infected COPD epithelial cells. Contrary to our results, Johansen et al. showed that COPD epithelial cells are much more susceptible to SARS-CoV-2 infection than healthy controls, which is associated with a stronger inflammatory response, potentially due to the overexpression of SARS-CoV-2 coreceptors, such as TMPRSS2 and a reduced anti-protease environment[36]. These findings could be attributed to various factors, notably the older age of the patients (76.5 years on average vs. 50.5 years in our study).

Overall, our *in vitro* epithelial model showed a weaker response to viral infection in the pathological epithelia of pwCF and patients with COPD suggesting that the initial inflammatory state of the epithelium protects against SARS-CoV-2 infection. Thus, during their lifetime, previous exposure of patients with COPD and CF to microorganisms, such as *P. aeruginosa* responsible for chronic inflammation, could condition their pulmonary response to subsequent SARS-CoV-2 infection. Indeed, prior exposure to pathogens could lead to distinct innate immune responses, such as trained immunity or tolerance[37] and our earlier work demonstrated that this phenomenon also occurs in lung epithelial cells *in vitro*[38]. Recent studies using COPD bronchial epithelial cells further support the existence of inflammatory memory linked to disease history[14]. Consistently, epidemiological data from patients with COPD and CF suggest that only a small proportion of these patients developed a severe form of COVID-19. However, a formal correlation between our *in vitro* results and epidemiological data could not be established. Recent work supports our hypothesis that in patients with COPD and CF, pulmonary inflammation preceding SARS-CoV-2 infection could explain the variability in response to SARS-CoV-2 infection. Indeed, studies using murine models demonstrated that activation of the pulmonary inflammatory response by respiratory pathogens, such as *Staphylococcus aureus*, which is associated with CF, Toll-Like receptor ligands, TNFα, or IL-1, establishes an antiviral state in the lungs, which limits SARS-CoV-2 replication[39].

CF and COPD share several overlapping phenotypic and pathological characteristics, suggesting potential mechanistic links. Both conditions are characterized by progressive airflow obstruction, persistent neutrophilic airway inflammation, and recurrent infectious exacerbations[40]. Notably, alterations in CFTR chloride channel function play a role in both diseases: genetically driven variants

in CF and dysfunction predominantly associated with cigarette smoke exposure in COPD[41]. Therapies targeting CFTR, proven effective in CF, as the potentiator ivacaftor are therefore garnering significant interest for potential applications in COPD[41]. This raises the question of whether the similar responses observed in CF and COPD epithelia to SARS-CoV-2 infection might be linked to CFTR dysfunction, and whether these phenotypes could be modulated by CFTR-targeting drugs. Pharmacological inhibition of CFTR using various CFTR inhibitors (inh-172, IOWH-032 and PPQ-102) has been shown to reduce SARS-CoV-2 infectivity and viral replication in bronchial epithelial cells[25,42]. However, a recent study on CF primary differentiated bronchial epithelial cells demonstrated that restoring CFTR activity with a combination of correctors (elexacaftor and tezacaftor) and the potentiator ivacaftor does not increase the susceptibility of CF epithelia to infection[24]. These contradictory results show that the specific role of both wild-type and mutated CFTR in the control of viral infection remains to be further investigated. It would thus be interesting to evaluate the role of CFTR activators in COPD cells that retain a non-mutated CFTR.

A limitation of our study is the use of donors of different ages in the three groups. The CF patient group was younger (mean age: 28 years) than the COPD (mean age: 50.5 years) and CTL (mean age: 45.75 years) groups. A recent study using nasal cells differentiated at the ALI showed that donor age plays an important role in the response to SARS-CoV-2, which is consistent with epidemiological data identifying age as a risk factor for severe COVID-19[43]. Donor age influences cell tropism; both ACE2 and TMPRSS2 expressions vary between paediatric (<12 years) and adult donors, as well as between adults of different ages (30–50 years vs. >70 years). The infected paediatric nasal epithelium shows high expression of IFN-stimulated genes and partial viral replication in goblet cells, whereas the infected older adult nasal epithelium shows an increase in basaloid-like cells, promoting viral spread and altering epithelial repair pathways. Although all donors were between 22–60 years of age (i.e. under 70 years), the effect of age between the CF and control groups could not be convincingly ruled out in our study.

In conclusion, the pre-existing inflammatory state of the airway epithelium in chronic respiratory diseases may paradoxically confer protection against severe COVID-19. This study provides important insights into the pathogenesis of SARS-CoV-2 infection and identifies potential biomarkers for clinical monitoring.

Resource availability

Lead Contact

Further information and requests for resources and reagents should be directed to and fulfilled by the lead contact Loic Guillot (loic.guillot@inserm.fr)

Material availability

The SARS-CoV-2 isolate generated in this study will be made available from Olivier Terrier (olivier.terrier@univ-lyon1.fr) with a completed Materials Transfer Agreement.

Data and code availability

The complete genome sequence of the isolated SARS-CoV-2 is available in the GISAID EpiCoVTM database. The RNA-Seq data were deposited to the ArrayExpress collection. The mass spectrometry proteomics data have been deposited to the ProteomeXchange Consortium via the PRIDE[44] partner repository. Accession numbers are listed in the key resources table.

Computer code is publically accessible through https://github.com/GENOM-IC-Cochin/RNA-Seq_analysis. Any additional information required to reanalyse the data reported in this paper is available from the lead contact upon reasonable request.

Limitation of the study

While we demonstrated that bronchial epithelium from healthy donors is significantly more sensitive to viral infection compared to that of CF or COPD donors—showing as a loss of epithelial integrity and elevated CXCL-10 production. it is important to note that this remains an in vitro model, which could not fully predict clinical reality at the individual level. Indeed, the age, sex and clinical variability of donors, which could not be tested, could influence the response of the reconstituted epithelium to SARS-COV-2. We identified a reduction in TMPRSS2 expression in CF cells, which may account for the apparent protection of the epithelium. However, the mechanisms underlying the reduced susceptibility of bronchial cells from COPD donors require further, more in-depth investigation.

Acknowledgements

The authors are grateful to Karine Bailly from the Cochin Cytometry and Immunobiology Facility; Lucie Adoux, Juliette Hamroune, Benjamin Saint-Pierre, and Franck Letourneur from the Cochin Genomi'C facility; Morgane Le Gall from the Cochin Protéomique 3P5 facility and to the Centre d'Imagerie Quantitative Lyon-Est (CIQLE) for providing access to the confocal microscopy platform. LG received a grant from the Faculté de Médecine Sorbonne Université (AAP COVID-19). OT received a grant from the Air Liquide Foundation (EpiCoV Project).

Author contributions

Conceptualisation: JO, MR, LG, OT; Methodology: JO, MR, SR, LG, OT; Investigation: JO, MR, CC, AG, AP, CG, SC, VAB, AS, AE, SR, HC, MRC, LG, OT; Writing – original draft: LG, OT; Writing Review & Editing, JO, MR, LG, OT, AP; Funding acquisition: LG, OT; Supervision: LG, OT.

Declaration of interests

The authors declare no competing interests.

Figure legends

Figure 1. **Severe acute respiratory syndrome coronavirus 2 (SARS-CoV-2) infection features in reconstituted bronchial human airway epithelium (HAE) obtained from control (CTL), chronic obstructive pulmonary disease (COPD), and cystic fibrosis (CF) donors**. **(A)** Summary of the experimental design: HAE obtained from four different donors for each group were mock-infected or infected with SARS-CoV-2 (multiplicity of infection [MOI] = 0.1) for 24, 48 or 72 h. Thus, to conduct the various analyses, the experiment includes two sets, each comprising a total of 72 HAE. At each timepoint, transepithelial electrical resistance (TEER; ohms.cm^2) was measured for the CTL **(B)**, CF **(C)**, and COPD **(D)** groups. Data are the mean (± SD) TEERs measured in each group, CTL, CF and COPD, each of which includes 4 donors. For each group, the number of values represented (n=8) corresponds to two independent measurements per individual (2 independent epithelium sets - see **Fig.**

1A). Two-way analysis of variance (ANOVA) was used with Sidak's multiple comparisons test. **(E)** Data are the mean (± SD) of the change in TEER between infected and mock condition and were determined at each timepoint for the three groups (n=8/group). Two-way ANOVA was used with Tukey's multiple comparisons test. Kinetics of (**F**) apical (relative to input as the reference=1) and (**G**) intracellular (relative to that of the housekeeping gene *GAPDH*) *nsp14* mRNA expression determined using quantitative reverse transcriptase-polymerase chain reaction. Data are the mean (± SD) of relative gene expression at each timepoint for the three groups (n=8/group). Two-way ANOVA was used with Tukey's multiple comparisons test. *, ** and **** for $p<0.05$, $p<0.01$ and $p<0.0001$, respectively. (**H**) Confocal images of mock-infected (left image) and SARS-CoV-2-infected HAE CTL cells (MOI = 0.1; 72 h) stained for ZO-1 (green) (middle image) and co-stained with the SARS-CoV-2 nucleocapsid (gradient) (overlay, right image). Nuclei were stained with DAPI (yellow). Images were taken at a magnification of ×63 (scale bar 50 μm).

Figure 2. Specific antiviral response in healthy (CTL) reconstituted bronchial HAE (A) Venn diagram depicting the total number of differentially expressed genes (DEGs) (padjBH<0.05, log2FC>1 and <-1, Base mean>20) in CTL HAE infected with SARS-CoV-2 (MOI=0.1) for 24, 48 or 72 h. **(B)** Heatmap of biological pathways involved in SARS-CoV-2 response of CTL HAE cells at 48 h and 72 h. **(C)** Volcano plot comparison of infected and mock-infected CTL cells (padjBH cut-off 1.3, log2FC cut-off: 1/-1). **(D-L)** Kinetics of IP-10 **(D)**, G-CSF **(E)**, RANTES **(F)**, IL-1β **(G)**, IFN-λ2 (IL-28B) **(H)**, TNF-α **(I)**, IL-17A **(J)**, IFN-γ **(K)**, IL-8 **(L)** production in CTL HAE cells infected with SARS-CoV-2 (MOI=0.1) for 24, 48 or 72 h. Data are the mean (± SD) of cytokine expression at each timepoint (n=4/group). *p<0.05 Two-way ANOVA was used with Sidak's multiple comparisons test. See **Fig. S1 and S2.**

Figure 3. Specific antiviral response in CF and COPD reconstituted bronchial HAE. **(A)** Venn diagram depicting the total number of DEGs (padjBH<0.05, log2FC>1 and <-1, Base mean>20) in CF HAE cells infected with SARS-CoV-2 (MOI=0.1) for 24, 48, or 72 h. **(B)** Heatmap of biological

pathways involved in SARS-CoV-2 response of CF HAE at 48 h and 72 h. **(C)** Volcano plot comparison of infected and mock-infected CF cells (padjBH cut-off 1.3, log2FC cut-off: 1/-1). **(D)** Kinetics of Matrix metalloproteinase-9 (MMP-9) production in CF HAE infected with SARS-CoV-2 (MOI=0.1) for 24, 48 or 72 h. Data are the mean (± SD) of MMP-9 expression at each timepoint (n=4/group). *p<0.05 Two-way ANOVA was used with Sidak's multiple comparisons test. **(E)** Venn diagram depicting the total number of DEGs (padjBH<0.05, log2FC>1 and <-1, Base mean>20) in COPD HAE infected with SARS-CoV-2 (MOI=0.1) for 24, 48, or 72 h. **(F)** Heatmap of biological pathways involved in SARS-CoV-2 response of COPD HAE at 48 h and 72 h. **(G)** Volcano plot comparison of infected and mock-infected COPD cells (padjBH cut-off 1.3, log2FC cut-off: 1/-1). **(H)** Kinetics of CXCL-10 production in COPD HAE infected with SARS-CoV-2 (MOI=0.1) for 24, 48, or 72 h. Data are the mean (± SD) of IP-10 expression at each timepoint (n=4/group). *p<0.05 Two-way ANOVA was used with Sidak's multiple comparisons test. See **Fig. S1 and S2.**

Figure 4. Comparison of transcriptomic signature of CTL, CF, and COPD reconstituted bronchial HAE with time. (A) Total number (up- and down-regulated) of DEGs in HAE from CF, COPD, and CTL donors infected with SARS-CoV-2 (MOI=0.1) for 24, 48, or 72 h. **(B)** Venn diagram depicting the total number of DEGs (padjBH<0.05, log2FC>1 and <-1, Base mean>20) in the CTL, CF, and COPD HAE infected with SARS-CoV-2 (MOI=0.1) for 48 or 72 h. **(C)** Heatmap of biological pathways involved in SARS-CoV-2 response of CTL, CF, and COPD HAE cells at 48 h and 72 h. (**D**) Venn diagram depicting the total number of DEGs (padjBH<0.05, log2FC>1 and <-1, Base mean>20) at 72 h among SARS-CoV-2-infected HAE from CTL, CF, and COPD groups. Gene Ontology enrichment analysis was performed with ShinyGO 0.8, using a list of specific DEGs (when the number of DEGs is sufficient). The charts represent the most enriched biological processes; the size and colour of the dots indicate the number of genes and the false discover rate (-log10(FDR)). **See Fig. S3 and S4.**

Figure 5. Comparison of inflammatory responses from CTL, CF, and COPD reconstituted bronchial HAE with time. Heatmap **(A)** (ClustVis options: clustering distance rows/columns:

correlation; Clustering method rows/columns: average) of mean comparative production data (Δ=differences between production measured without and with infection in each group; n=4) with time (24, 48, or 72 h) of inflammatory mediators, including IP-10 **(B)** between CTL, CF, and COPD HAE infected with SARS-CoV-2 (MOI=0.1) at each timepoint. **p<0.01, ***p<0.001 Two-way ANOVA was used with Tukey's multiple comparisons test. **(C)** Kinetic of ΔsICAM-1 (infected/non-infected) mean (± SD) expression using enzyme-linked immunosorbent assay (ELISA) in bronchial epithelial cells from CTL, CF, and COPD groups (n=4/group) infected with SARS-CoV-2 (MOI=0.1) for 24, 48, and 72 h. *p<0.05 Two-way ANOVA was used with Tukey's multiple comparisons test. **(D)** Kinetics of sICAM-1 mean (± SD) expression using ELISA in mock-infected or SARS-CoV-2-infected (MOI=0.1) CTL group (n=4) at 24, 48 and 72h. *p<0.05 Two-way ANOVA was used with Sidak's multiple comparisons test **(E)** ICAM-1 mRNA (mean number (n) ± SD of reads, extracted RNAseq data) **(F)** and protein (relative expression after normalization against β-actin) expressions in CF, COPD, and CTL HAE (n=4/group) infected with SARS-CoV-2 (MOI=0.1) for 72 h. *p<0.05 paired t-test. See **Fig. S6.**

Figure 6. Comparison of transcriptomic and proteomic signatures of initial infection-free states among CTL, CF, and COPD reconstituted bronchial HAE. (A) Venn diagram depicting the total number of DEGs among non-infected CTL, CF, and COPD HAE at 24 h (padjBH<0.05). **(B)** Heatmap of biological pathways involved in the initial infection-free state of CTL, CF, and COPD HAE at 24 h. **(C)** Volcano plot for comparison of protein expressions between non-infected CF and CTL HAE at 24 h (padjBH cut-off 1.3, log2FC cut-off: 1.5/-1.5). **(D)** Network (STRING) of predicted associations of the proteins coded by the 86 differentially expressed proteins between non-infected CF and CTL HAE cells at 24 h. The network nodes are proteins, and the edges represent the predicted functional associations. Line thickness indicates the strength of data support. Four clusters (K-means clustering) have been identified (light and dark green, red and blue). **(E)** Temporal comparison of the mean (± SD) expressions of various transcripts among CTL, CF, and COPD HAE (n=4/group) in uninfected or SARS-COV-2-infected conditions (*padjBH<0.05: uninfected (-) vs. (+) SARS-CoV-2;

(#padjBH<0.05: CF vs. CTL or COPD vs. CTL at 24h uninfected; $padjBH<0.05: CF vs. COPD at 24 h uninfected). **(F)** Angiotensin-converting enzyme 2 (ACE2) and TMPRSS2 mRNA (mean number (n) (± SD) of reads, extracted RNAseq data, padjBH<0.05) and **(G)** protein expressions in CTL, CF, and COPD HAE (n=4/group) not infected at 24h. Data are the mean (± SD) of relative TMPRSS2 and ACE2 protein expressions after normalization against GAPDH. One-way analysis of variance (ANOVA) was used with Tukey's multiple comparisons test. **(H)** TMPRSS2 activity in HAE cells from two CTL (n=9 independent inserts per donor), one CF donor (n=9 independent inserts) and one COPD donor (n=9 independent inserts) treated or not with camostat mesylate (n=3 independent inserts for each donor). *p<0.05, ***p<0.001, ****p<0.0001; One-way analysis of variance (ANOVA) was used with Sidak's multiple comparisons test.

Figure 7. Violin plot of expression levels (z-scores) of IP-10, sICAM-1, SERPINA1, SERPINA3, C3, C4, and CFB proteins between COVID+ and COVID- patients (**A**), severe and moderate COVID+ patients (**B**) and COVID+ and COVID- patients with COPD (**C**).

Supplemental information:

Tables S1–S6 and Figures S1-S6

STAR Methods

KEY RESOURCES TABLE

EXPERIMENTAL MODEL AND STUDY PARTICIPANT DETAILS

Reconstituted bronchial HAE

HAE were obtained from bronchi samples of healthy individuals (control: CTL, 4 independent donors including 2 males and 2 females), patients diagnosed with COPD (n=4 independent donors including 2 males and 2 females), and pwCF (4 independent donors including 2 males and 2 females), all of whom

were homozygous for the F508del variant; these were provided by Epithelix SARL (MucilAir™, Plan-les-Ouates, Switzerland; see **Key Ressources Table** for specific donors details). These cells were cultured simultaneously at an ALI for 3 weeks to allow differentiation. Subsequently, the HAE were cultured in MucilAir™ culture medium at 37 °C, 5% CO_2 (Epithelix), following the manufacturer's instructions. All the HAE were certified by Epithelix negative for mycoplasma. Considering the known risk factors for severe COVID-19, the experimental design included as many male and female donors for the healthy and pathological groups. As expected, owing to the intrinsic characteristics of CF, pwCF (mean age: 28 years) were younger than those with COPD (mean age: 50.5; p=0.043, Tukey's multiple comparison test) and CTL (mean age: 45.75, not significant). These studies were conducted in accordance with the Declaration of Helsinki on Biomedical Research (Hong Kong amendment, 1989) and approved by the local ethics commission. This project was approved (Opinion number 20-688/20-688 bis) by the Inserm Institutional Review Board (IRB00003888, IORG0003254, FWA00005831).

Epithelial cell lines

Pr Dieter Gruenert (originator) and Dr Beate Illek (provider) from the University of California San Francisco generously supplied 16HBE14o- (16HBE) cells. The cells were cultured in minimum essential medium-Glutamax supplemented with 10 % FCS and 1 % antibiotics, as recommended by the manufacturer. Cells with the *CFTR* variants (F508del, G551D, G542X and W1282X) were obtained from the Cystic Fibrosis Foundation and cultured as recommended by the manufacturer [45]. 16HBE cells were negative for mycoplasma contamination (MycoStrip™, Invivogen, Toulouse, France).

Virus

The SARS-CoV-2 strain used was isolated from a 47-year-old female patient enrolled in a French clinical cohort of patients with COVID-19 (NCT04262921)[10]. Sequence deposited in the GISAID EpiCoVTM database under BetaCoV/France/IDF0571/2020 (accession ID EPI_ISL_411218).

BCQ19 cohort

The circulating proteome of BQC19 patients was analyzed between 2 April 2020 and 20 April 2021 using a multiplex SOMAmer affinity array (SomaLogic, 4,985 aptamers). The data were pre-processed according to the protocol described in a previous study[46]. A two-sided Mann–Whitney U test was used to assess the association between the levels of these mediators and disease characteristics.

METHOD DETAILS

SARS-CoV-2 infection and viral quantification

All experiments involving clinical samples and manipulation of infectious SARS-CoV-2 were performed in biosafety level 3 facilities, using the appropriate protocols. Two sets of HAE cells from CTL (n=4), COPD (n=4), and CF (n=4) were washed gently twice with OptiMEM (Life technologies, Paisley, UK)) at the apical poles and then were mock-infected (OptiMEM) or infected with SARS-CoV-2 (strain BetaCoV/France/IDF0571/2020; accession ID EPI_ISL_411218) with a multiplicity of infection of 0.1, as previously described (1 h of contact with the virus followed by a change in medium) [10] for 24, 48, and 72 h at 37 °C, 5% CO_2 (**Fig. 1A**). Apical washes and basal media were collected at each timepoint and conserved at -80 °C for further analysis. HAE cells were harvested in cell lysis buffer, and total RNA was extracted for subsequent real-time quantitative reverse transcriptase and polymerase chain reaction (RT-qPCR) and RNA-seq analysis.

SARS-CoV-2 quantification

Viral quantification in the apical media was performed using the EXPRESS One-Step Superscript RT-qPCR Kit (Invitrogen, Carlsbad, CA, USA) (Set 1) and primer and probe sequences targeting the ORF1b-nsp14 as previously detailled[10]. The relative expression level of ORF1b-nsp14 was expressed relative to the input.

Intracellular quantification of *ORF1b-nsp14* and *GAPDH* (housekeeping HAE gene) was perfomed by RT-qPCR of the total RNA extracted from cell lysates (Set 1) using the NucleoSpin RNA/miRNA kit (Macherey Nagel, Duren, Germany). RT and PCR were performed using a high-capacity cDNA kit (Applied Biosystems, Foster City, CA, USA) and a Sensifast Probe Lo-Rox Kit (Bio-Technofix,

Guibeville, France) respectively. Thermal cycling was performed using an ABI QS3 apparatus (Applied Biosystems, Foster City, CA, USA). The relative expression level of *ORF1b-nsp14* was normalized to the expression of *GAPDH* relative to the reference group (not infected) used as a calibrator and was calculated using the $2^{-\Delta\Delta Ct}$ method.

TEER Measurement

TEER was measured at each timepoint (in sets 1 and 2) using an Epithelial Volt/Ohm meter (EVOM2, World precision instrument, Hitchin Hertfordshire, UK) and expressed as $Ohm.cm^2$.

Immunofluorescence

Mock- and SARS-CoV-2-infected cells were fixed with 4% PFA for 10 min and permeabilized (1X PBS containing 0.1% Triton X-100) through two 25-min incubations, targeting both the apical and basal surfaces. Blocking was carried out by incubating the cells with 1X PBS supplemented with 1% FBS applied to both surfaces. For immunolabeling, the apical surface was incubated for 2 h with primary antibodies against the SARS-CoV-2 nucleoprotein and the tight junction marker ZO-1. Afterward, cells underwent three 10 min washes with 1X PBS containing 0.1% Triton X-100, followed by a 30 min incubation with secondary antibodies applied to the apical surface. Post-secondary antibody staining, three additional 10 min washes with 1X PBS containing 0.1% Triton X-100 were performed. Nuclei were stained with DAPI at a concentration of 1 µg/mL for 10 min, followed by two final 10 min washes with 1X PBS. The epithelial monolayers were subsequently mounted on slides using Fluoromount (Invitrogen, 00-4958-02). Confocal images were acquired using a Leica TCS-SP5X imaging system (Wetzlar, Germany).

Reverse Transcription-quantitative polymerase chain reaction

RNA from 16HBE14o- cells was extracted using the NucleoSpin RNA kit (Macherey Nagel) and RT was performed using a high-capacity cDNA reverse transcription kit (Applied Biosystems). Real-time qPCR was performed as described above using TaqMan probes (Applied Biosystems) for *GAPDH, C3*

and *CFB*. *GAPDH* was used to normalize the expression levels of the target genes. The relative expression of each gene was calculated using a reference group and the $2^{-\Delta\Delta Ct}$ method.

Transcriptomic study

RNA from Set 1 was isolated using a NucleoSpin RNA/miRNA kit (Macherey-Nagel, Duren, Germany), and quantified using a fluorometric Qubit RNA assay (Life Technologies, Grand Island, New York, USA). RNA quality (RNA integrity number, RIN) was determined using an Agilent 2100 Bioanalyzer (Agilent Technologies, Palo Alto, CA, USA), according to the manufacturer's instructions. Two samples CTL- SARS-CoV-2-72 h and COPD-CTL-24 h, did not meet the quality criteria (RIN <7) and were excluded. To construct the libraries, 400 ng of high-quality total RNA was processed using a TruSeq Stranded mRNA kit (Illumina), according to the manufacturer's instructions. Libraries were quantified using qPCR with the KAPA Library Quantification Kit for Illumina Libraries (Kapa Biosystems, Wilmington, MA, USA), and library profiles were assessed using the DNA High Sensitivity LabChip kit on an Agilent Bioanalyzer. Libraries were sequenced on an Illumina NextSeq 500 instrument using 75 base-lengths read V2 chemistry in the paired-end mode. After sequencing, a primary analysis based on AOZAN software (ENS, Paris) was applied to the demultiplex to control the quality of the raw data (based on FastQC modules/version 0.11.5). The obtained fastq files were then aligned using the STAR algorithm (version 2.5.2b), and quality control of the alignment was performed using Picard tools (version 2.8.1). Reads were then counted using Featurecount (version Rsubread 1.24.1), and statistical analyses of the read counts were performed using the DESeq2 package version 1.14.1, to determine the proportion of DEGs among the experimental groups. Venn diagrams were constructed using Jvenn[47] and Volcano plots using VolcaNoseR[48]. Enrichment analysis was performed using ShinyGo[49] and Metascape[50].

Protein extraction and western blot

Protein extracts (20 µg, set 2) in radioimmunoprecipitation assay buffer supplemented with anti-protease-antiphosphatase (Halt™ Protease and Phosphatase Inhibitor Single-Use Cocktail, Thermo Fisher Scientific, Waltham, USA) were reduced and size-separated on 4–15% Mini-PROTEAN® TGX

Stain-Free™ Precast Gels (Bio-Rad, Hercules, CA, USA) and transferred onto nitrocellulose membranes using an iBlot2™ Gel Transfer Device and iBlot2™ Nitrocellulose Regular Stacks (IB23001, Invitrogen). Membranes were incubated with primary antibodies followed by secondary-horseradish peroxidase antibody. Immunodetection was performed using Clarity Western ECL Substrate (#170-5061, Bio-Rad). Images were acquired using a Las-3000 system (Fujifilm, Bussy-Saint-Georges, France). Densitometric quantification was performed using the ImageJ software (https://imagej.net).

Proteomic analysis

Protein digestion

Ten micrograms of each sample (set 2) was diluted 1:1 with 2× lysis buffer [10% (w/v) SDS in 100 mM triethylammonium bicarbonate (TEAB), pH 8.5] and incubated for 10 min in an ultrasonic bath. Disulfide bridges were reduced using 20 mM dithiothreitol treatment for 10 min at 90 °C and subsequently alkylated with 40 mM iodoacetamide for 30 min in the dark. Lysates were then transferred into S-TRAP microspin columns (Protifi), according to the manufacturer's instructions. Samples were then digested with 1 µg trypsin (sequencing-grade modified trypsin, Promega) overnight at 37 °C. Peptides were collected in three successive elution steps using 50 mM TEAB, 0.2% (v/v) formic acid (FA), and 50% (v/v) acetonitrile (ACN) in 0.2% (v/v) formic acid. All the elutes were then dried in a vacuum centrifuge (Speed-Vac, Thermo Scientific) and resuspended in 20 µL 2% (v/v) acetonitrile and 0.1% (v/v) formic acid. Desalting of the peptides was performed on an automated platform (DigestProMSi, CEM, Matthews, North Carolina, USA), with in-house packed StageTips and two layers of C18 medium (Empore C18). The eluted peptides were dried in SpeedVac and resuspended in 2% acetonitrile and 0.1% formic acid before mass spectrometric (MS) analysis.

Liquid chromatography-tandem mass spectrometry

The peptide mixtures were analysed using a NanoElute UHPLC system (Bruker, Bremen, Germany) coupled to a timeTOF Pro mass spectrometer (Bruker). Peptides were separated on an analytical column RP-C18 Aurora 2 (25 cm, 75 µm i.d., 120 Å, 1.6 µm - IonOpticks, Fitzroy, Australia) at a flow rate of

250 nL/min, at 50 °C, with mobile phase A (0.1 % FA) and B (99.9 % ACN / 0.1 % FA). The elution gradient was as follows: 2–13% B for 42 min, 13–20% B for 23 min, and 20–30% B for 5 min, for a total time of 70 min. MS acquisition was performed in the DIA-PASEF mode. The accumulation time was set as 100 ms for the TIMS tunnel. Capillary voltage and temperature were set at 1.6 kV and 180 °C respectively. The mass ranges for MS1 were set to *m/z* 100 – 1700. The dia-PASEF window scheme ranged in dimension m/z from 343 to 1036 and in dimension 1/K0 0.7–1.2, with 21 windows of 33 m/z with a ramp time of 100 ms, for a total cycle time of 1.06 seconds. The maximum window height was 0.2 1/K0. The collision energy was decreased as a function of the ion mobility (IM) from 59 eV at 1/K0 = 1.6 V cm^{-2} to 20 eV at 1/K0 = 0.6 V cm^{-2}. The IM dimension was calibrated using three Agilent ESI Tuning Mix ions (m/z, 1/K0:622.02, 0.9915 V cm^{-2}, 922.01, 1.1986 V cm^{-2}, 1221.99, and 1.3934 V cm^{-2}).

Data analysis

DIA-PASEF data files were analysed using DIA-NN[51] version 1.8.1. For constructing the spectral library, the SwissProt *Homo sapiens* reference proteome (UP000005640, release 2023-02 with 20598 entries) was used as the reference database. For *in silico* digestion, trypsin/P specificity was chosen with only one missed cleavage allowed. N-terminal methionine excision, methionine oxidation, and N-terminal acetylation were accepted as variable peptide modifications, with a maximum of one modification per sequenced peptide, whereas cysteine carbamidomethylation was set as a fixed modification. The peptide length range was set to 7–30 residues, spanning a charge state range of 2–4. The precursor m/z range was set to 300–1700 and the fragment m/z range was set to 200–1700. MS1 and MS2 mass accuracies were set to 15 and 14 ppm, respectively. Protein inference was performed at the gene level and heuristic protein inference was enabled. The feature of match-between-runs was activated. RT-dependent cross-run normalisation and robust LC (high precision) options were selected for quantification. Enrichment analysis was performed using STRING [52].

Differential expression analysis

All differential expression analyses were performed using ProStaR software suite, version 1.28.0 [53]. First, all DIA-NN results were loaded into the software; entries related to contaminants and reversed sequences were excluded from the dataset, resulting in 7936 entries. Imputation of partially observed values and missing in the entire condition values was performed using the Det Quantile algorithm in a quantile of 2.5 and a factor of 1. Following imputation, the ProStaR false discovery rate calibration tool (adaptive Benjamini-Hochberg algorithm) and Limma statistical test were used to determine significant differences between the experimental groups. All results were exported and the list of differentially expressed proteins was manually assessed.

Inflammatory protein quantification

The inflammatory response was quantified in basal media (set 1). The molecules were measured using a Human Magnetic Luminex Assay (R&D Systems). The panel included C-Reactive Protein (CRP), CCL2 (MCP-1), CCL5 (RANTES), CXCL2 (MIP-2), CXCL-10 (IP-10), Furin, G-CSF, sICAM-1, IFN-β, IFN-γ, IL-1α/IL-1F1, IL-1β/IL-1F2, IL-6, IL-17/IL-17A, IL-17C, IL-17E/IL-25, IL-28A/IFN-λ2, IL-28B/IFN-λ3, MMP-1, MMP-2, MMP-9, Neuropilin-1, S100A9, and TNF-α. IL-8 concentrations were measured using an ELISA kit (DY208; R&D Systems, Minneapolis, MN, USA), according to the manufacturer's instructions. The substrate 3,3′,5,5′-tetramethylbenzidine was procured from Cell Signalling Technology (Danvers, MA, USA). A heat map of the inflammatory response was generated using ClustVis[54].

TMPRSS2 activity

A fluorogenic substrate assay was performed to examine TMPRSS2 catalytic activity[55,56]. Bronchial HAE obtained from CTL (n=12) and pwCF (n=12) were incubated with a fluorogenic peptide substrate (Boc-Gln-Ala-Arg-AMC; Ref ES014; R&D Systems Minneapolis, MN, USA, 200 mM in Opti-MEM) at 37 °C, 5% CO2 for 1 h. The fluorescence intensity was monitored using a microplate reader (Spark multimode microplate reader, Tecan) at 380/460 nm emission/excitation wavelengths. As a control, for each group of HAE, three epitheliums were pre-treated for 24 h with Camostat mesylate (Ref 3193;

R&D Systems Minneapolis, MN, USA, 40 µM in basal medium) which is a serine protease inhibitor effective against TMPRSS2 [57].

Clinical datasets and pre-processing

The circulating proteome of BQC19 patients was measured between 2 April 2020 and 20 April 2021 using a multiplex SOMAmer affinity array (SomaLogic, 4,985 aptamers). When measurements of the same patients at different time points were available, we used data corresponding to the first time point. The SomaScan is a biotechnological protocol commercialised by SomaLogic. This relies on a set of artificial aptamers linked to a fluorophore, each designed to bind a single protein. Once added to the sample, the activity of each aptamer was measured using fluorescence and was used to determine the approximate target protein expression level. The SomaScan protocol comprises several levels of calibration and normalisation to correct technical biases (summarised in our previous study[46]). Log2 and Z-score normalisation were performed on each aptamer separately, in addition to the normalised data provided by the manufacturer (hybridisation control normalisation, intraplate median signal normalisation, and median signal normalisation). As the data were analysed using SomaLogic in two separate batches, we applied the z-score transformation separately to each batch to reduce batch effects. These additional transformations ensured that the measured values of the different aptamers were comparable and could be used for cluster analysis.

Ethics

This project was approved (Opinion number 20-688/20-688 bis) by the Inserm Institutional Review Board (IRB00003888, IORG0003254, FWA00005831)

QUANTIFICATION AND STATISTICAL ANALYSIS

Apart from RNA-seq and proteomic data, differences among groups were assessed for statistical significance using Prism 10.00 software (GraphPad Software, La Jolla, CA, USA) as indicated in the figure legends. $P < 0.05$ was considered statistically significant.

Table S1. Effect of infection in CTL group over time. Related to Figure 2. List of DEGs (24, 48, and 72 h) following SARS-CoV-2 infection in the CTL reconstituted bronchial human airway epithelium (HAE) group overtime. Selection criteria: p<0.05; Log2FC<-1 >1; Base mean>20). Red: Upregulated DEGs; Blue: downregulated DEGs.

Table S2. Effect of infection in CF group over time. Related to Figure 3. List of DEGs (24, 48, and 72 h) following SARS-CoV-2 infection in the CF reconstituted bronchial (HAE) group overtime. Selection criteria: p<0.05; Log2FC<-1 >1; Base mean>20). Red: Upregulated DEGs; Blue: downregulated DEGs.

Table S3. Effect of infection in COPD group over time. Related to Figure 3. List of DEGs (24, 48, and 72h) following SARS-CoV-2 infection in the COPD reconstituted bronchial (HAE) group overtime. Selection criteria: p<0.05; Log2FC<-1 >1; Base mean>20). Red: Upregulated DEGs; Blue: downregulated DEGs.

Table S4. Comparison of infected groups over time. Related to Figure 4 and Figure S4. List of DEGs after SARS-CoV-2 infection between CF and COPD reconstituted bronchial HAE and the CTL HAE groups overtime (24, 48, and 72 h). Selection criteria: p<0.05; Log2FC<-1 >1; Base mean>20). Red: Upregulated DEGs; Blue: downregulated DEGs.

Table S5. Comparison of groups by effect of infection. Related to Figure S5. List of DEGs 72 h after SARS-CoV-2 infection in CF and COPD reconstituted bronchial HAE versus the CTL group, considering the initial uninfected state. Selection criteria: p<0.05; Log2FC<-1 >1; Base mean>20). Red: Upregulated DEGs; Blue: downregulated DEGs.

Table S6. **Comparison of uninfected groups over time – genes. Related to Figure 6.** List of DEGs between the non-infected reconstituted bronchial HAE of the pathological groups (CF or COPD) and the CTL group overtime (24, 48, and 72 h). Selection criteria: p<0.05; Log2FC<-1 >1; Base mean>20. Red: Upregulated DEGs; Blue: downregulated DEGs.

Table S7. Comparison of uninfected groups at 24h – proteins. Related to Figure 6. List of proteins differentially expressed between uninfected CF and CTL reconstituted bronchial HAE at 24 h.

References

1. Zhang, J.J., Dong, X., Liu, G.H., and Gao, Y.D. (2023). Risk and Protective Factors for COVID-19 Morbidity, Severity, and Mortality. Clin Rev Allergy Immunol *64*, 90-107. 10.1007/s12016-022-08921-5.
2. Conway, F.M., Bloom, C.I., and Shah, P.L. (2022). Susceptibility of Patients with Airway Disease to SARS-CoV-2 Infection. Am J Respir Crit Care Med *206*, 696-703. 10.1164/rccm.202111-2547PP.
3. Naehrlich, L., Orenti, A., Dunlevy, F., Kasmi, I., Harutyunyan, S., Pfleger, A., Keegan, S., Daneau, G., Petrova, G., Tjesic-Drinkovic, D., et al. (2021). Incidence of SARS-CoV-2 in people with cystic fibrosis in Europe between February and June 2020. J Cyst Fibros *20*, 566-577. 10.1016/j.jcf.2021.03.017.
4. Corvol, H., de Miranda, S., Dehillotte, C., Lemonnier, L., Chiron, R., Danner-Boucher, I., Hamidfar, R., Houdouin, V., Macey, J., Marguet, C., et al. (2022). Cumulative Incidence and Risk Factors for Severe Coronavirus Disease 2019 in French People With Cystic Fibrosis. Clin Infect Dis *75*, 2135-2144. 10.1093/cid/ciac333.
5. Gerayeli, F.V., Milne, S., Cheung, C., Li, X., Yang, C.W.T., Tam, A., Choi, L.H., Bae, A., and Sin, D.D. (2021). COPD and the risk of poor outcomes in COVID-19: A systematic review and meta-analysis. EClinicalMedicine *33*, 100789. 10.1016/j.eclinm.2021.100789.
6. Alqahtani, J.S., Oyelade, T., Aldhahir, A.M., Alghamdi, S.M., Almehmadi, M., Alqahtani, A.S., Quaderi, S., Mandal, S., and Hurst, J.R. (2020). Prevalence, Severity and Mortality associated with COPD and Smoking in patients with COVID-19: A Rapid Systematic Review and Meta-Analysis. PLoS One *15*, e0233147. 10.1371/journal.pone.0233147.
7. Aveyard, P., Gao, M., Lindson, N., Hartmann-Boyce, J., Watkinson, P., Young, D., Coupland, C.A.C., Tan, P.S., Clift, A.K., Harrison, D., et al. (2021). Association between pre-existing respiratory disease and its treatment, and severe COVID-19: a population cohort study. Lancet Respir Med *9*, 909-923. 10.1016/S2213-2600(21)00095-3.
8. Sunjaya, A.P., Allida, S.M., Di Tanna, G.L., and Jenkins, C.R. (2022). Asthma and COVID-19 risk: a systematic review and meta-analysis. Eur Respir J *59*. 10.1183/13993003.01209-2021.
9. Chua, R.L., Lukassen, S., Trump, S., Hennig, B.P., Wendisch, D., Pott, F., Debnath, O., Thurmann, L., Kurth, F., Volker, M.T., et al. (2020). COVID-19 severity correlates with airway epithelium-immune cell interactions identified by single-cell analysis. Nat Biotechnol *38*, 970-979. 10.1038/s41587-020-0602-4.
10. Pizzorno, A., Padey, B., Julien, T., Trouillet-Assant, S., Traversier, A., Errazuriz-Cerda, E., Fouret, J., Dubois, J., Gaymard, A., Lescure, F.X., et al. (2020). Characterization and Treatment of SARS-

CoV-2 in Nasal and Bronchial Human Airway Epithelia. Cell Rep Med *1*, 100059. 10.1016/j.xcrm.2020.100059.

11. Gold, L., Ayers, D., Bertino, J., Bock, C., Bock, A., Brody, E.N., Carter, J., Dalby, A.B., Eaton, B.E., Fitzwater, T., et al. (2010). Aptamer-based multiplexed proteomic technology for biomarker discovery. PLoS One *5*, e15004. 10.1371/journal.pone.0015004.
12. Robinot, R., Hubert, M., de Melo, G.D., Lazarini, F., Bruel, T., Smith, N., Levallois, S., Larrous, F., Fernandes, J., Gellenoncourt, S., et al. (2021). SARS-CoV-2 infection induces the dedifferentiation of multiciliated cells and impairs mucociliary clearance. Nat Commun *12*, 4354. 10.1038/s41467-021-24521-x.
13. Wiszniewski, L., Jornot, L., Dudez, T., Pagano, A., Rochat, T., Lacroix, J.S., Suter, S., and Chanson, M. (2006). Long-term cultures of polarized airway epithelial cells from patients with cystic fibrosis. Am J Respir Cell Mol Biol *34*, 39-48. 10.1165/rcmb.2005-0161OC.
14. Carlier, F.M., Detry, B., Lecocq, M., Collin, A.M., Plante-Bordeneuve, T., Gerard, L., Verleden, S.E., Delos, M., Rondelet, B., Janssens, W., et al. (2024). The memory of airway epithelium damage in smokers and COPD patients. Life Sci Alliance *7*. 10.26508/lsa.202302341.
15. Hao, S., Ning, K., Kuz, C.A., Vorhies, K., Yan, Z., and Qiu, J. (2020). Long-Term Modeling of SARS-CoV-2 Infection of In Vitro Cultured Polarized Human Airway Epithelium. mBio *11*. 10.1128/mBio.02852-20.
16. Zarkoob, H., Allue-Guardia, A., Chen, Y.C., Garcia-Vilanova, A., Jung, O., Coon, S., Song, M.J., Park, J.G., Oladunni, F., Miller, J., et al. (2022). Modeling SARS-CoV-2 and influenza infections and antiviral treatments in human lung epithelial tissue equivalents. Commun Biol *5*, 810. 10.1038/s42003-022-03753-7.
17. Liu, M., Guo, S., Hibbert, J.M., Jain, V., Singh, N., Wilson, N.O., and Stiles, J.K. (2011). CXCL10/IP-10 in infectious diseases pathogenesis and potential therapeutic implications. Cytokine Growth Factor Rev *22*, 121-130. 10.1016/j.cytogfr.2011.06.001.
18. Gudowska-Sawczuk, M., and Mroczko, B. (2022). What Is Currently Known about the Role of CXCL10 in SARS-CoV-2 Infection? Int J Mol Sci *23*. 10.3390/ijms23073673.
19. Cheemarla, N.R., Hanron, A., Fauver, J.R., Bishai, J., Watkins, T.A., Brito, A.F., Zhao, D., Alpert, T., Vogels, C.B.F., Ko, A.I., et al. (2023). Nasal host response-based screening for undiagnosed respiratory viruses: a pathogen surveillance and detection study. Lancet Microbe *4*, e38-e46. 10.1016/S2666-5247(22)00296-8.
20. Rajagopala, S.V., Strickland, B.A., Pakala, S.B., Kimura, K.S., Shilts, M.H., Rosas-Salazar, C., Brown, H.M., Freeman, M.H., Wessinger, B.C., Gupta, V., et al. (2022). Mucosal gene expression in response to SARS-CoV-2 is associated with early viral load. bioRxiv. 10.1101/2022.08.23.504908.
21. Yang, Y., Shen, C., Li, J., Yuan, J., Wei, J., Huang, F., Wang, F., Li, G., Li, Y., Xing, L., et al. (2020). Plasma IP-10 and MCP-3 levels are highly associated with disease severity and predict the progression of COVID-19. J Allergy Clin Immunol *146*, 119-127 e114. 10.1016/j.jaci.2020.04.027.
22. Baresi, G., Giacomelli, M., Moratto, D., Chiarini, M., Conforti, I.C., Padoan, R., Poli, P., Timpano, S., Caldarale, F., and Badolato, R. (2021). Case Report: Analysis of Inflammatory Cytokines IL-6, CCL2/MCP1, CCL5/RANTES, CXCL9/MIG, and CXCL10/IP10 in a Cystic Fibrosis Patient Cohort During the First Wave of the COVID-19 Pandemic. Front Pediatr *9*, 645063. 10.3389/fped.2021.645063.
23. Lotti, V., Merigo, F., Lagni, A., Di Clemente, A., Ligozzi, M., Bernardi, P., Rossini, G., Concia, E., Plebani, R., Romano, M., et al. (2022). CFTR Modulation Reduces SARS-CoV-2 Infection in Human Bronchial Epithelial Cells. Cells *11*. 10.3390/cells11081347.
24. Pagani, I., Venturini, A., Capurro, V., Nonis, A., Ghezzi, S., Lena, M., Alcala-Franco, B., Gianferro, F., Guidone, D., Colombo, C., et al. (2024). Distinct Responses of Cystic Fibrosis Epithelial Cells to SARS-CoV-2 and Influenza A Virus. Am J Respir Cell Mol Biol. 10.1165/rcmb.2024-0213OC.

25. Bezzerri, V., Gentili, V., Api, M., Finotti, A., Papi, C., Tamanini, A., Boni, C., Baldisseri, E., Olioso, D., Duca, M., et al. (2023). SARS-CoV-2 viral entry and replication is impaired in Cystic Fibrosis airways due to ACE2 downregulation. Nat Commun *14*, 132. 10.1038/s41467-023-35862-0.
26. Tukiainen, T., Villani, A.C., Yen, A., Rivas, M.A., Marshall, J.L., Satija, R., Aguirre, M., Gauthier, L., Fleharty, M., Kirby, A., et al. (2017). Landscape of X chromosome inactivation across human tissues. Nature *550*, 244-248. 10.1038/nature24265.
27. Carraro, G., Langerman, J., Sabri, S., Lorenzana, Z., Purkayastha, A., Zhang, G., Konda, B., Aros, C.J., Calvert, B.A., Szymaniak, A., et al. (2021). Transcriptional analysis of cystic fibrosis airways at single-cell resolution reveals altered epithelial cell states and composition. Nat Med *27*, 806-814. 10.1038/s41591-021-01332-7.
28. Wettstein, L., Weil, T., Conzelmann, C., Muller, J.A., Gross, R., Hirschenberger, M., Seidel, A., Klute, S., Zech, F., Prelli Bozzo, C., et al. (2021). Alpha-1 antitrypsin inhibits TMPRSS2 protease activity and SARS-CoV-2 infection. Nat Commun *12*, 1726. 10.1038/s41467-021-21972-0.
29. Henke, M.O., John, G., Germann, M., Lindemann, H., and Rubin, B.K. (2007). MUC5AC and MUC5B mucins increase in cystic fibrosis airway secretions during pulmonary exacerbation. Am J Respir Crit Care Med *175*, 816-821. 10.1164/rccm.200607-1011OC.
30. Kulkarni, H.S., Elvington, M.L., Perng, Y.C., Liszewski, M.K., Byers, D.E., Farkouh, C., Yusen, R.D., Lenschow, D.J., Brody, S.L., and Atkinson, J.P. (2019). Intracellular C3 Protects Human Airway Epithelial Cells from Stress-associated Cell Death. Am J Respir Cell Mol Biol *60*, 144-157. 10.1165/rcmb.2017-0405OC.
31. Afzali, B., Noris, M., Lambrecht, B.N., and Kemper, C. (2022). The state of complement in COVID-19. Nat Rev Immunol *22*, 77-84. 10.1038/s41577-021-00665-1.
32. Mastellos, D.C., Hajishengallis, G., and Lambris, J.D. (2023). A guide to complement biology, pathology and therapeutic opportunity. Nat Rev Immunol. 10.1038/s41577-023-00926-1.
33. Tam, J.C., Bidgood, S.R., McEwan, W.A., and James, L.C. (2014). Intracellular sensing of complement C3 activates cell autonomous immunity. Science *345*, 1256070. 10.1126/science.1256070.
34. Sahu, S.K., Ozanturk, A.N., Kulkarni, D.H., Ma, L., Barve, R.A., Dannull, L., Lu, A., Starick, M., McPhatter, J., Garnica, L., et al. (2023). Lung epithelial cell-derived C3 protects against pneumonia-induced lung injury. Sci Immunol *8*, eabp9547. 10.1126/sciimmunol.abp9547.
35. Santos, L., Nascimento, R., Duarte, A., Railean, V., Amaral, M.D., Harrison, P.T., Gama-Carvalho, M., and Farinha, C.M. (2023). Mutation-class dependent signatures outweigh disease-associated processes in cystic fibrosis cells. Cell Biosci *13*, 26. 10.1186/s13578-023-00975-y.
36. Johansen, M.D., Mahbub, R.M., Idrees, S., Nguyen, D.H., Miemczyk, S., Pathinayake, P., Nichol, K., Hansbro, N.G., Gearing, L.J., Hertzog, P.J., et al. (2022). Increased SARS-CoV-2 Infection, Protease, and Inflammatory Responses in Chronic Obstructive Pulmonary Disease Primary Bronchial Epithelial Cells Defined with Single-Cell RNA Sequencing. Am J Respir Crit Care Med *206*, 712-729. 10.1164/rccm.202108-1901OC.
37. Divangahi, M., Aaby, P., Khader, S.A., Barreiro, L.B., Bekkering, S., Chavakis, T., van Crevel, R., Curtis, N., DiNardo, A.R., Dominguez-Andres, J., et al. (2021). Trained immunity, tolerance, priming and differentiation: distinct immunological processes. Nat Immunol *22*, 2-6. 10.1038/s41590-020-00845-6.
38. Bigot, J., Guillot, L., Guitard, J., Ruffin, M., Corvol, H., Chignard, M., Hennequin, C., and Balloy, V. (2020). Respiratory Epithelial Cells Can Remember Infection: A Proof-of-Concept Study. J Infect Dis *221*, 1000-1005. 10.1093/infdis/jiz569.
39. Baker, P.J., Bohrer, A.C., Castro, E., Amaral, E.P., Snow-Smith, M., Torres-Juarez, F., Gould, S.T., Queiroz, A.T.L., Fukutani, E.R., Jordan, C.M., et al. (2024). The inflammatory microenvironment of the lung at the time of infection governs innate control of SARS-CoV-2 replication. Sci Immunol *9*, eadp7951. 10.1126/sciimmunol.adp7951.
40. De Rose, V., Molloy, K., Gohy, S., Pilette, C., and Greene, C.M. (2018). Airway Epithelium Dysfunction in Cystic Fibrosis and COPD. Mediators Inflamm *2018*, 1309746. 10.1155/2018/1309746.

41. Mall, M.A., Criner, G.J., Miravitlles, M., Rowe, S.M., Vogelmeier, C.F., Rowlands, D.J., Schoenberger, M., and Altman, P. (2023). Cystic fibrosis transmembrane conductance regulator in COPD: a role in respiratory epithelium and beyond. Eur Respir J *61*. 10.1183/13993003.01307-2022.
42. Lagni, A., Lotti, V., Diani, E., Rossini, G., Concia, E., Sorio, C., and Gibellini, D. (2023). CFTR Inhibitors Display In Vitro Antiviral Activity against SARS-CoV-2. Cells *12*. 10.3390/cells12050776.
43. Woodall, M.N.J., Cujba, A.M., Worlock, K.B., Case, K.M., Masonou, T., Yoshida, M., Polanski, K., Huang, N., Lindeboom, R.G.H., Mamanova, L., et al. (2024). Age-specific nasal epithelial responses to SARS-CoV-2 infection. Nat Microbiol *9*, 1293-1311. 10.1038/s41564-024-01658-1.
44. Perez-Riverol, Y., Bai, J., Bandla, C., Garcia-Seisdedos, D., Hewapathirana, S., Kamatchinathan, S., Kundu, D.J., Prakash, A., Frericks-Zipper, A., Eisenacher, M., et al. (2022). The PRIDE database resources in 2022: a hub for mass spectrometry-based proteomics evidences. Nucleic Acids Res *50*, D543-D552. 10.1093/nar/gkab1038.
45. Valley, H.C., Bukis, K.M., Bell, A., Cheng, Y., Wong, E., Jordan, N.J., Allaire, N.E., Sivachenko, A., Liang, F., Bihler, H., et al. (2019). Isogenic cell models of cystic fibrosis-causing variants in natively expressing pulmonary epithelial cells. J Cyst Fibros *18*, 476-483. 10.1016/j.jcf.2018.12.001.
46. Ma, W., Soulé, A., Liu, K.Y., Allard, C., Qureshi, S., Tremblay, K., Rousseau, S., and Emad, A. (2022). Molecular stratification of hospitalized COVID19 patients points to FGFR and SHC4-signaling in ARDS. medRxiv, 2022.2011.2002.22281834. 10.1101/2022.11.02.22281834.
47. Bardou, P., Mariette, J., Escudie, F., Djemiel, C., and Klopp, C. (2014). jvenn: an interactive Venn diagram viewer. BMC Bioinformatics *15*, 293. 10.1186/1471-2105-15-293.
48. Goedhart, J., and Luijsterburg, M.S. (2020). VolcaNoseR is a web app for creating, exploring, labeling and sharing volcano plots. Sci Rep *10*, 20560. 10.1038/s41598-020-76603-3.
49. Ge, S.X., Jung, D., and Yao, R. (2020). ShinyGO: a graphical gene-set enrichment tool for animals and plants. Bioinformatics *36*, 2628-2629. 10.1093/bioinformatics/btz931.
50. Zhou, Y., Zhou, B., Pache, L., Chang, M., Khodabakhshi, A.H., Tanaseichuk, O., Benner, C., and Chanda, S.K. (2019). Metascape provides a biologist-oriented resource for the analysis of systems-level datasets. Nat Commun *10*, 1523. 10.1038/s41467-019-09234-6.
51. Demichev, V., Messner, C.B., Vernardis, S.I., Lilley, K.S., and Ralser, M. (2020). DIA-NN: neural networks and interference correction enable deep proteome coverage in high throughput. Nat Methods *17*, 41-44. 10.1038/s41592-019-0638-x.
52. Szklarczyk, D., Kirsch, R., Koutrouli, M., Nastou, K., Mehryary, F., Hachilif, R., Gable, A.L., Fang, T., Doncheva, N.T., Pyysalo, S., et al. (2023). The STRING database in 2023: protein-protein association networks and functional enrichment analyses for any sequenced genome of interest. Nucleic Acids Res *51*, D638-D646. 10.1093/nar/gkac1000.
53. Wieczorek, S., Combes, F., Lazar, C., Giai Gianetto, Q., Gatto, L., Dorffer, A., Hesse, A.M., Coute, Y., Ferro, M., Bruley, C., and Burger, T. (2017). DAPAR & ProStaR: software to perform statistical analyses in quantitative discovery proteomics. Bioinformatics *33*, 135-136. 10.1093/bioinformatics/btw580.
54. Metsalu, T., and Vilo, J. (2015). ClustVis: a web tool for visualizing clustering of multivariate data using Principal Component Analysis and heatmap. Nucleic Acids Res *43*, W566-570. 10.1093/nar/gkv468.
55. Zhang, Y., Sun, S., Du, C., Hu, K., Zhang, C., Liu, M., Wu, Q., and Dong, N. (2022). Transmembrane serine protease TMPRSS2 implicated in SARS-CoV-2 infection is autoactivated intracellularly and requires N-glycosylation for regulation. J Biol Chem *298*, 102643. 10.1016/j.jbc.2022.102643.
56. Shapira, T., Monreal, I.A., Dion, S.P., Buchholz, D.W., Imbiakha, B., Olmstead, A.D., Jager, M., Desilets, A., Gao, G., Martins, M., et al. (2022). A TMPRSS2 inhibitor acts as a pan-SARS-CoV-2 prophylactic and therapeutic. Nature *605*, 340-348. 10.1038/s41586-022-04661-w.

57. Kawase, M., Shirato, K., van der Hoek, L., Taguchi, F., and Matsuyama, S. (2012). Simultaneous treatment of human bronchial epithelial cells with serine and cysteine protease inhibitors prevents severe acute respiratory syndrome coronavirus entry. J Virol *86*, 6537-6545. 10.1128/JVI.00094-12.

Figure 1

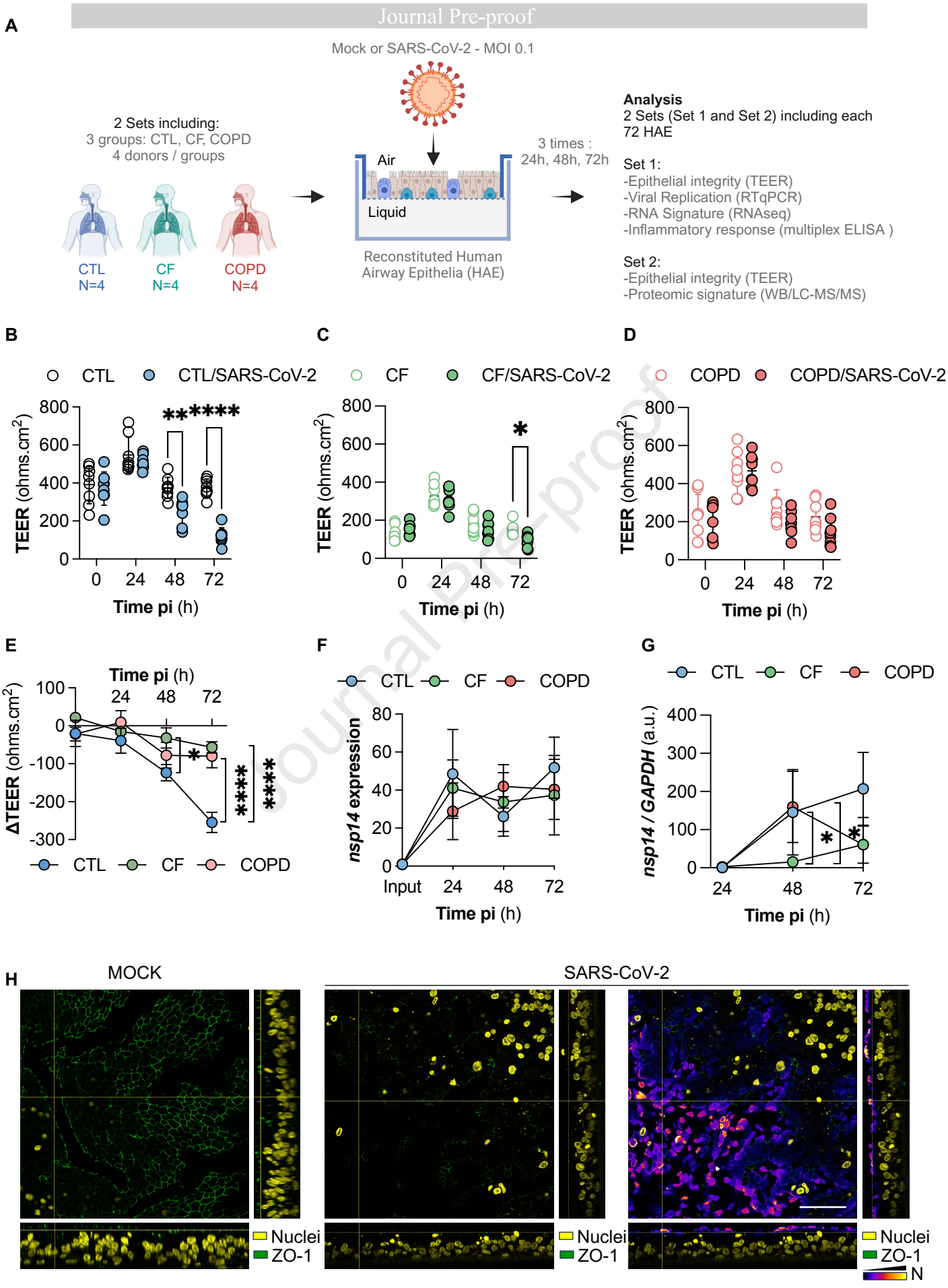

Figure 2

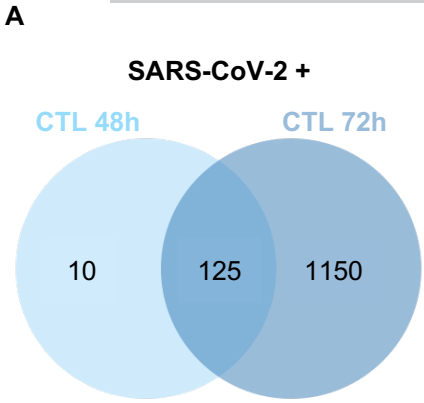

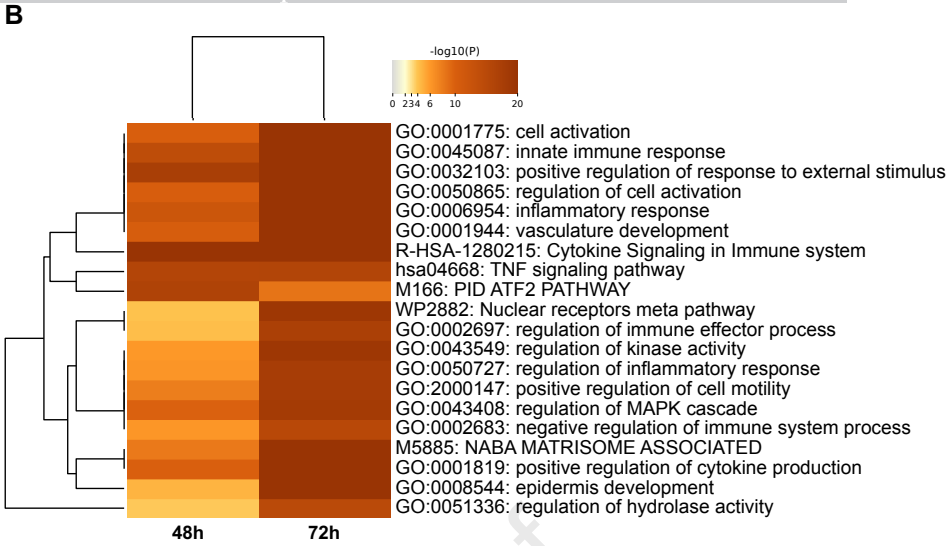

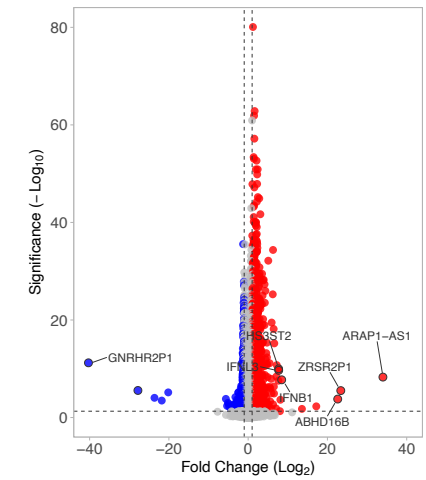

Genes	Log2FC	padjBH
IFNB1	8,46	1,83E-08
IFNL3	7,70	2,10E-10
IFNL1	7,21	1,78E-11
IFNL2	7,10	4,03E-09
C11orf96	6,43	6,86E-19
DNAJC27-AS1	-2,24	6,39E-05
OR7C1	-2,46	7,52E-06
AMIGO3	-2,52	0,001
DISP2	-4,11	0,004
GET1-SH3BGR	-4,23	0,037

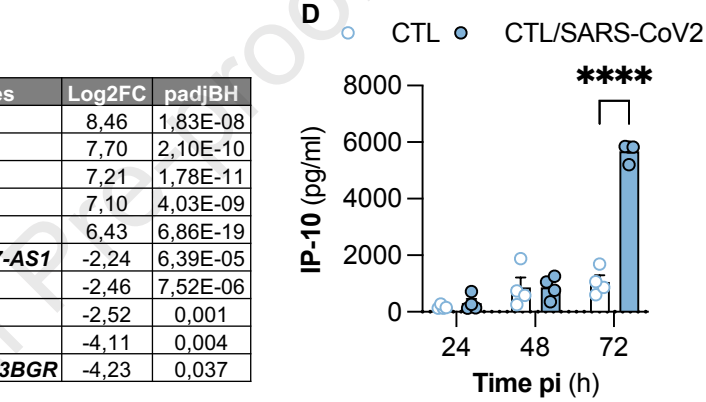

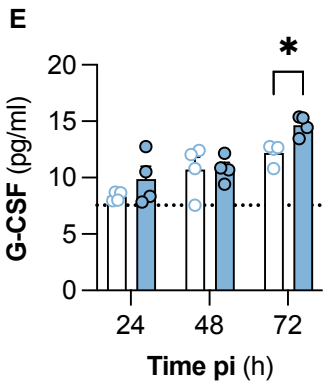

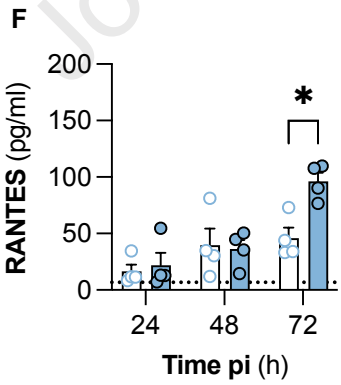

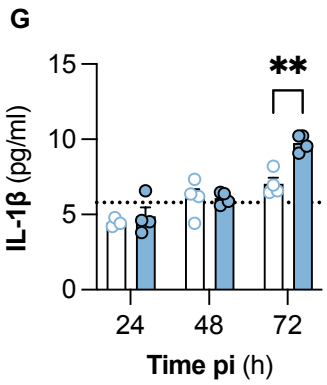

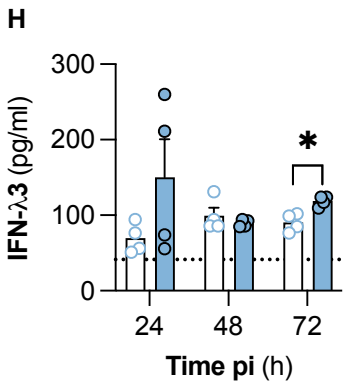

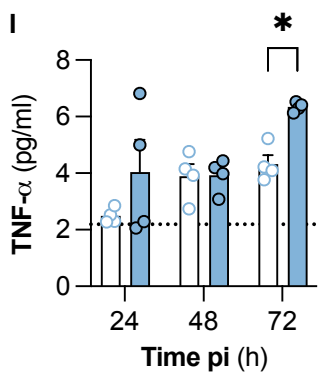

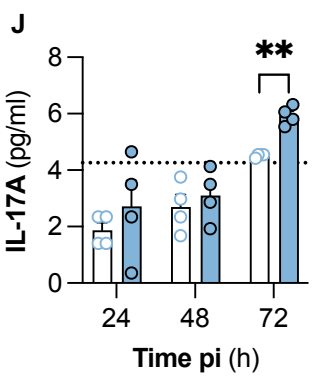

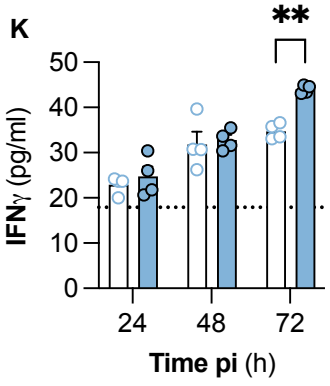

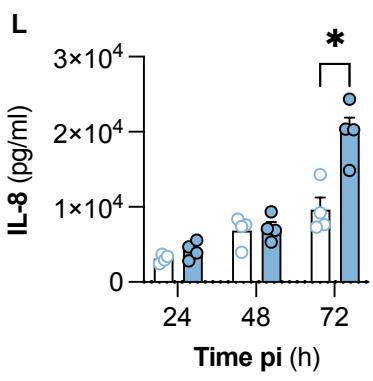

Figure 3

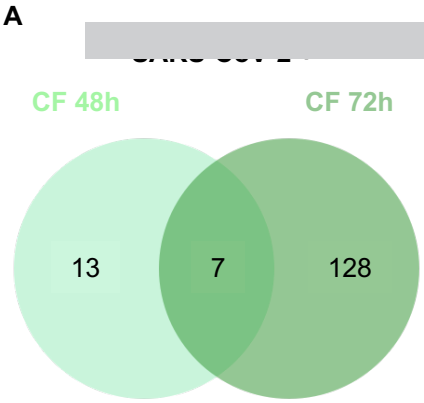

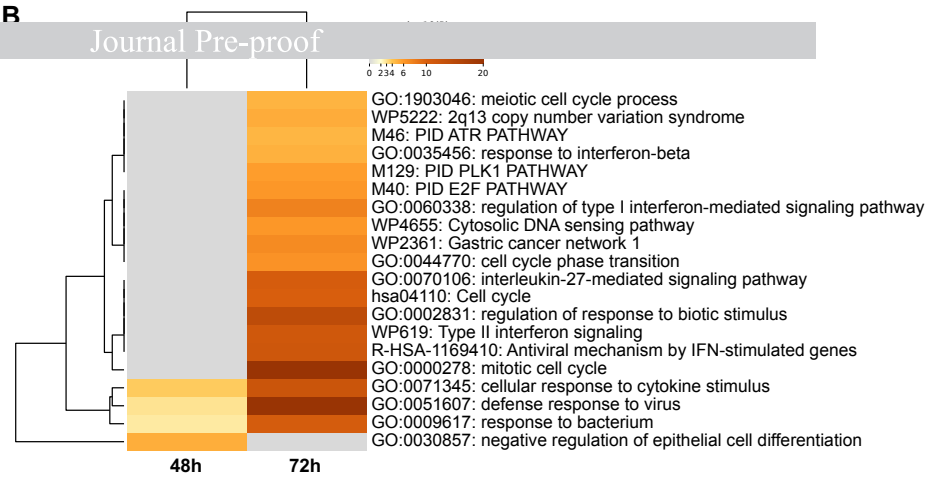

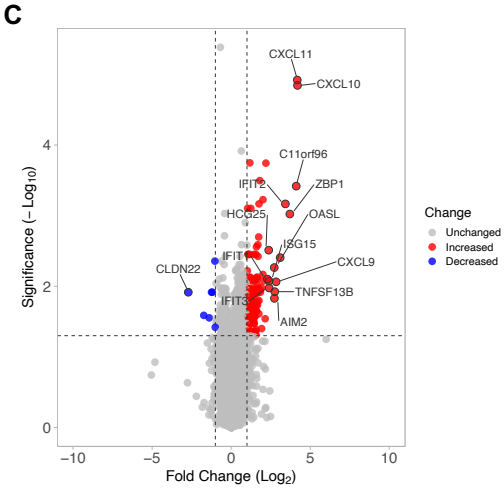

Genes	Log2FC	padjBH
CXCL10	4,19	1,43E-05
CXCL11	4,18	1,20E-05
C11orf96	4,11	0,0004
ZBP1	3,71	0,0009
IFIT2	3,43	0,0007
PDE11A	-1,19	0,0121
SAP30-DT	-1,24	0,0121
LRRC8C-DT	-1,39	0,0280
NAIPP2	-1,73	0,0258
CLDN22	-2,71	0,0121

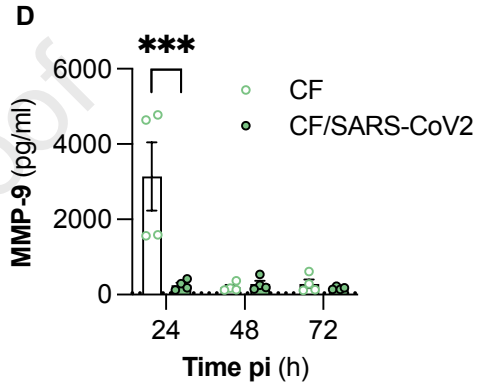

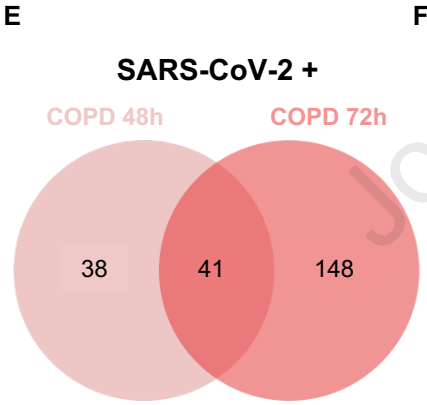

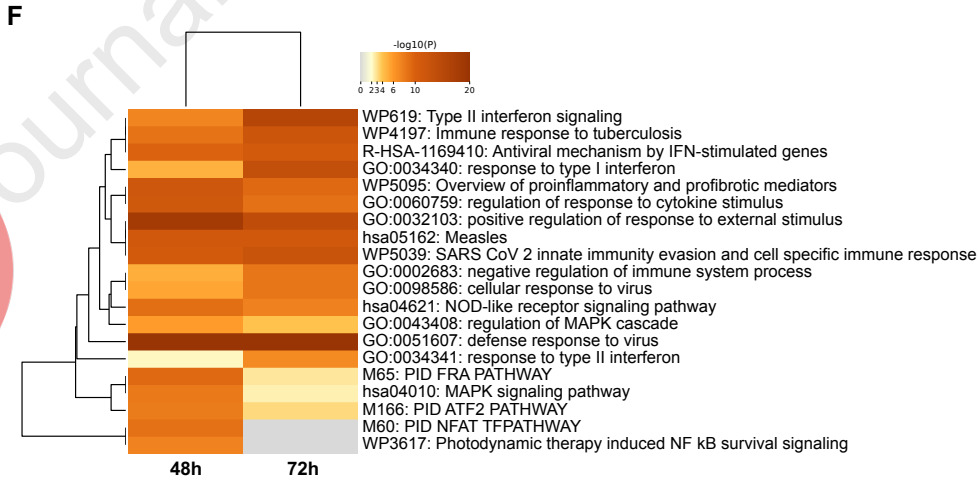

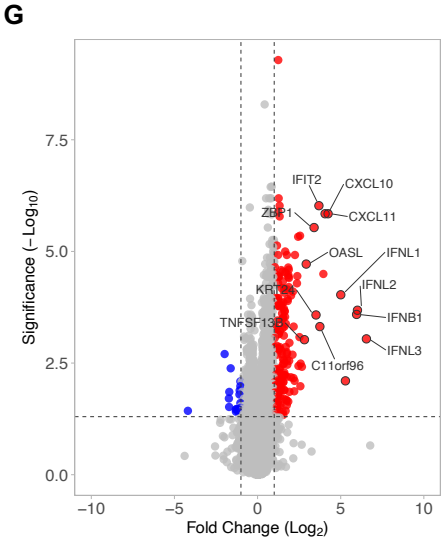

Genes	Log2FC	padjBH
IFNL3	6,54	0,0009
IFNL2	6	0,0002
IFNB1	5,95	0,0002
IFNL1	5	9,34E-05
CXCL11	4,24	1,43E-06
SCN8A	-1,3	0,0346
ADAM19	-1,61	0,0041
FGF1	-1,70	0,014
LINC01220	-1,71	0,0304
AGAP7P	-1,72	0,0196

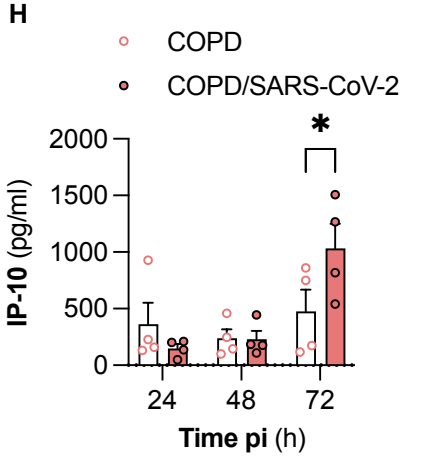

Figure 4

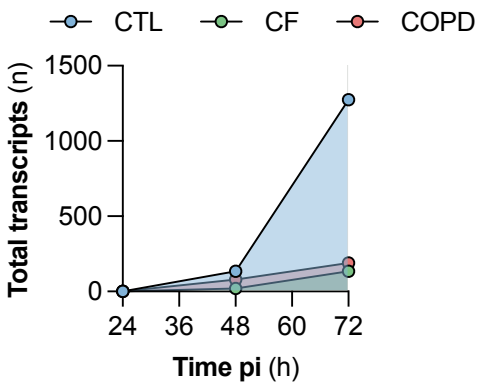

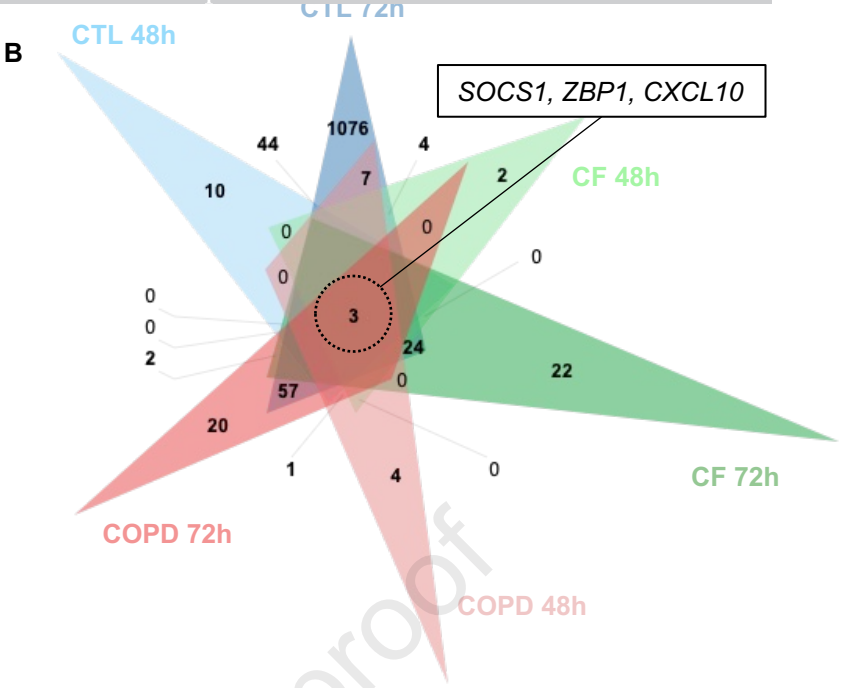

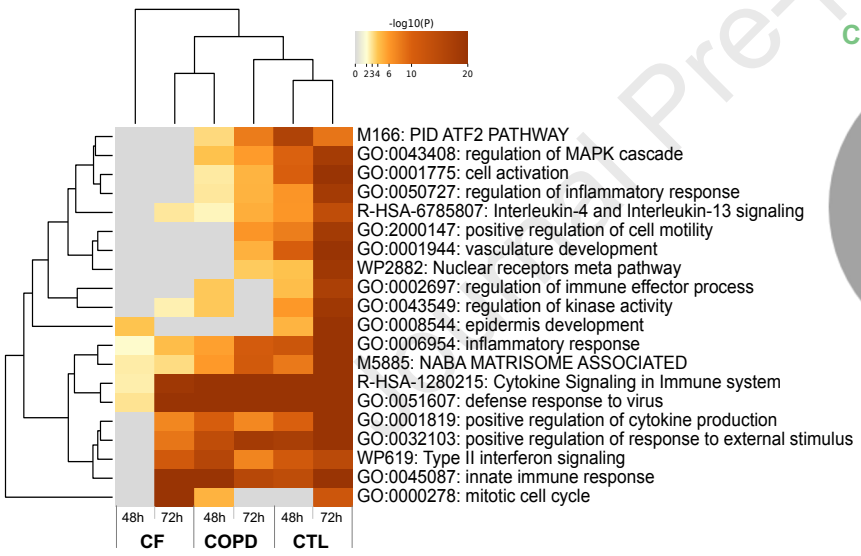

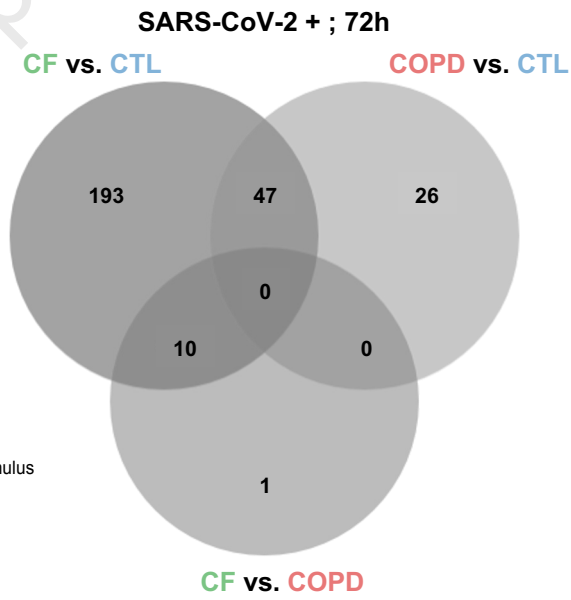

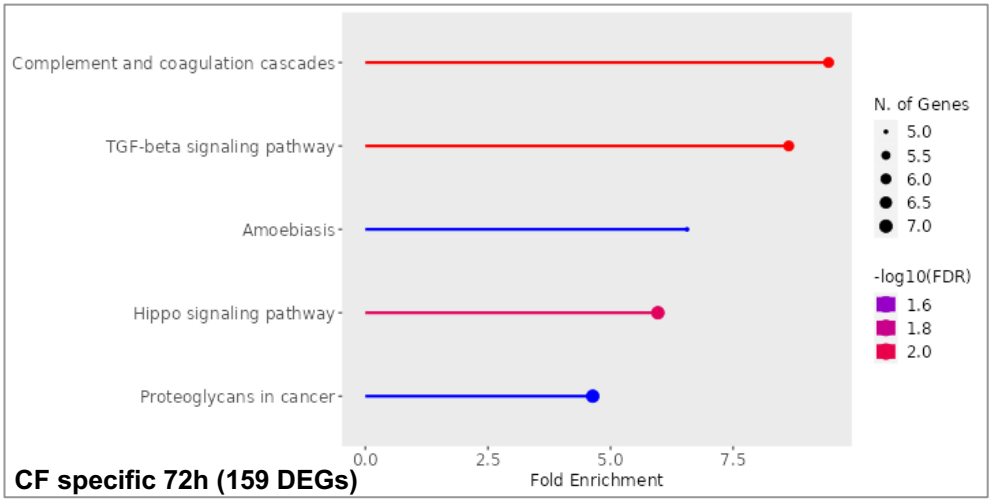

Figure 5

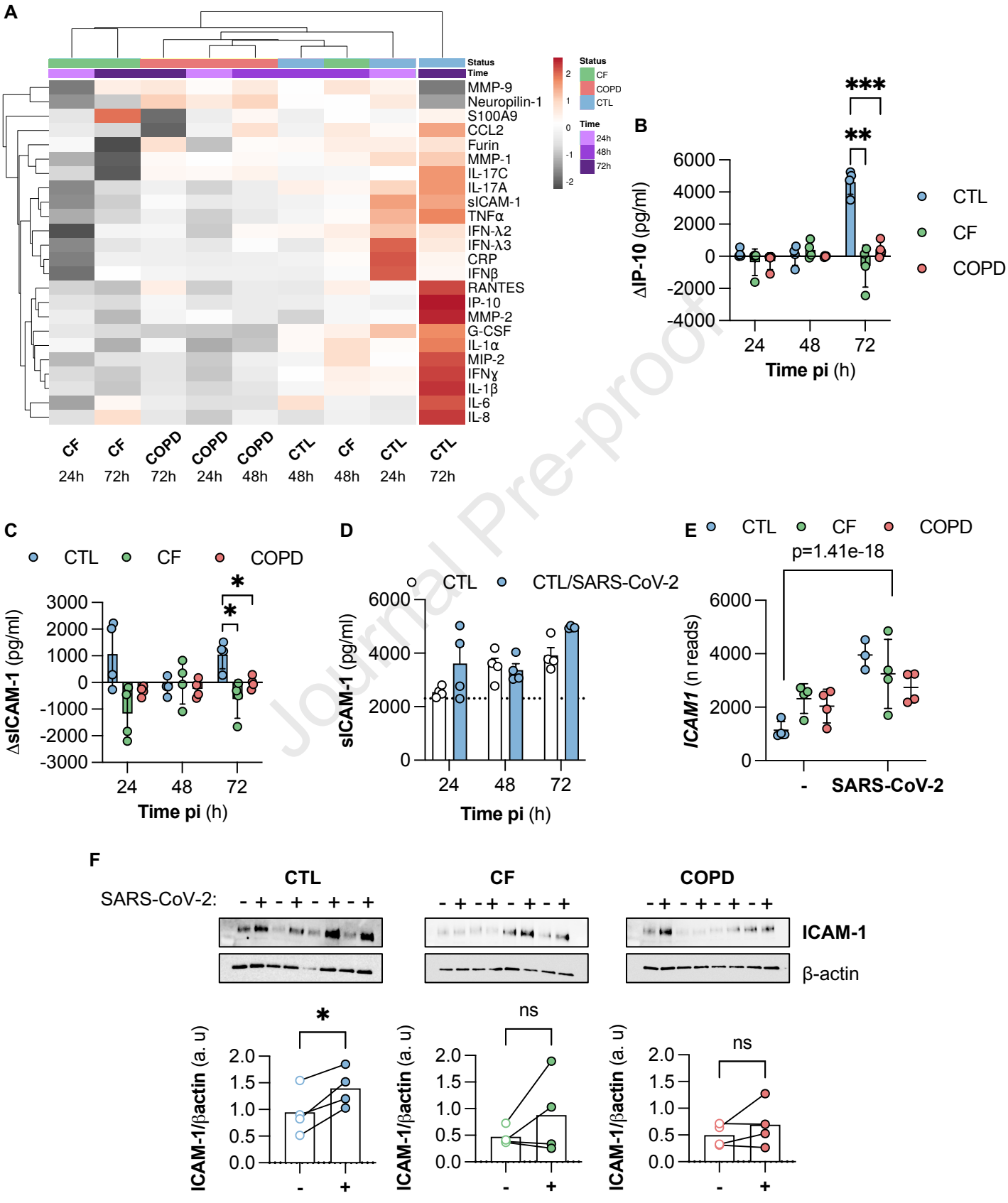

Figure 6

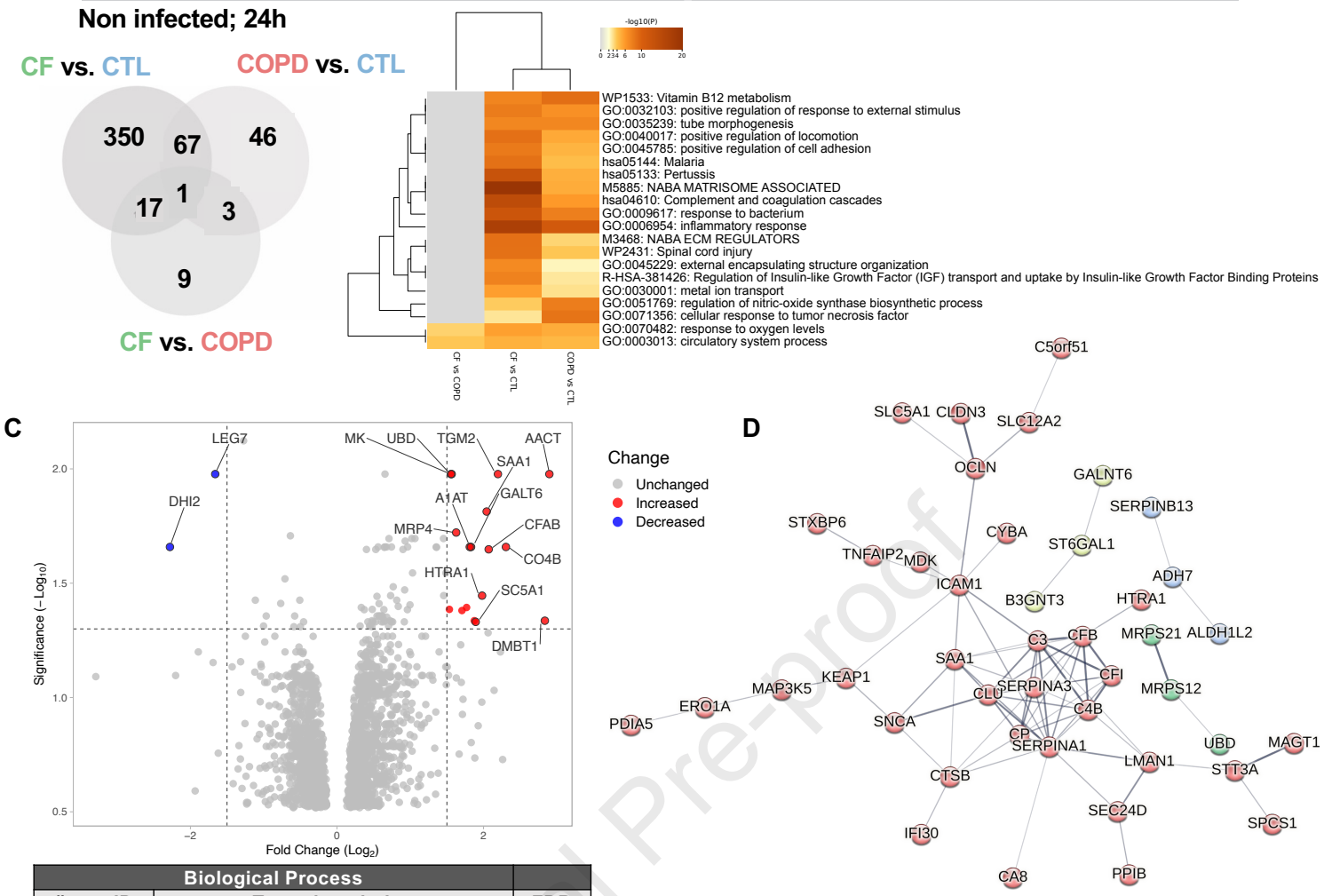

Biological Process		
#term ID	Term description	FDR
GO:0052547	Regulation of peptidase activity	0.0104
GO:0010466	Negative regulation of peptidase activity	0.0143
GO:0030162	Regulation of proteolysis	0.0222
GO:0006956	Complement activation	0.0364

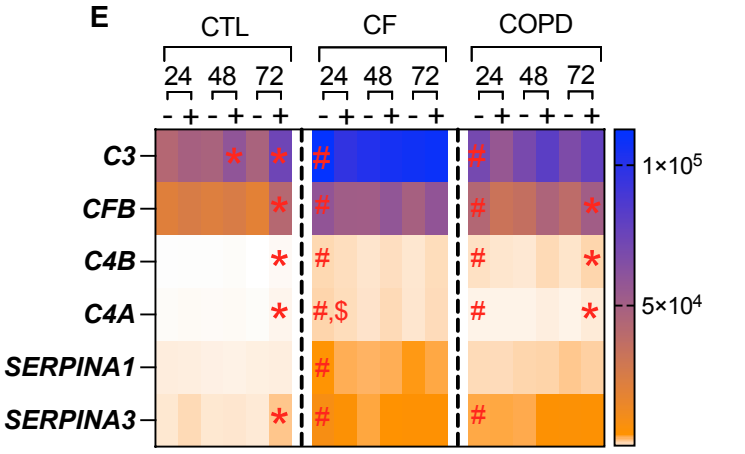

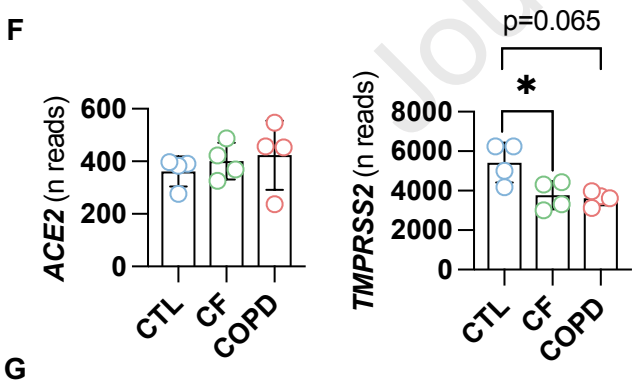

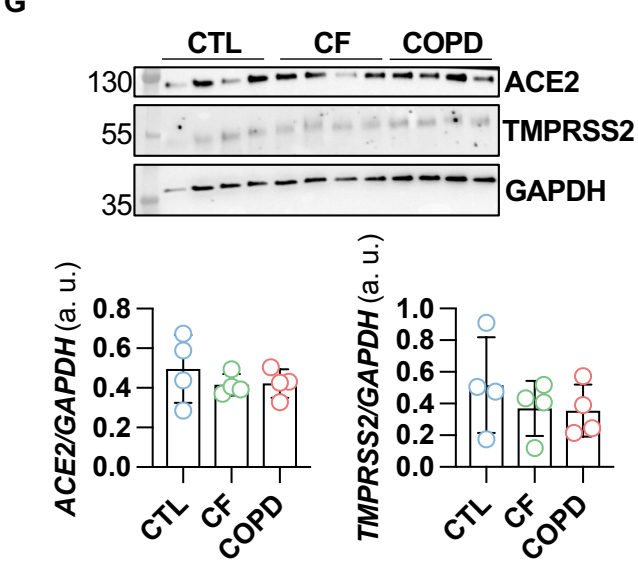

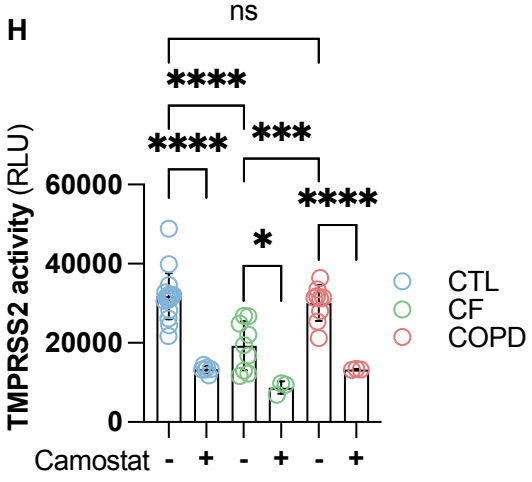

Figure 7

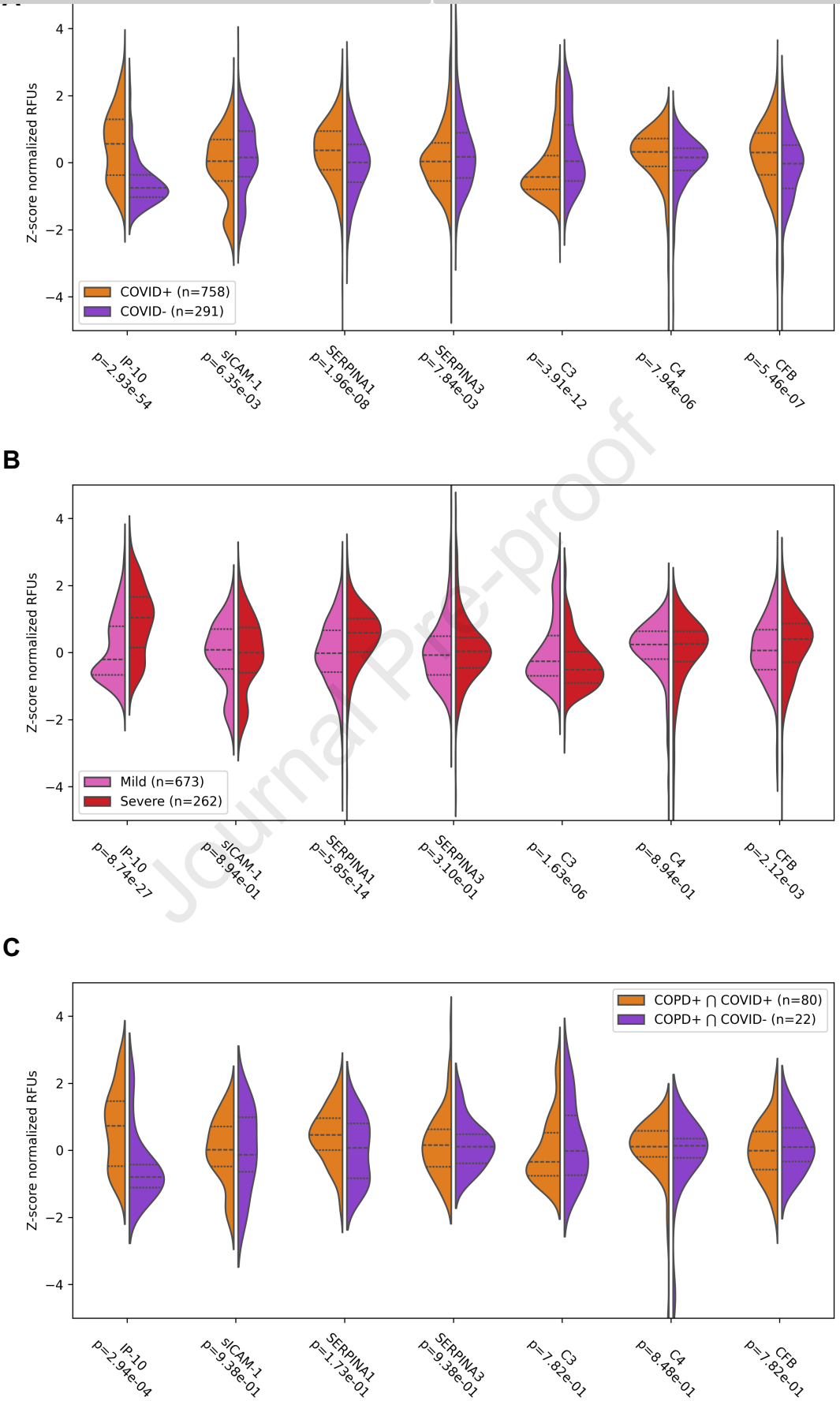

Highlights

- CF and COPD airway epithelia showed reduced susceptibility to SARS-CoV-2
- Reduced TMPRSS2 activity was observed in the CF epithelium post-infection.
- Specific inflammatory markers correlate with COVID-19 severity
- This study elucidates SARS-CoV-2 pathogenesis and potential clinical biomarkers

KEY RESOURCES TABLE

REAGENT or RESOURCE	SOURCE	IDENTIFIER
Antibodies		
Anti-ICAM-1 (1/1000)	Proteintech	Cat#10831-1-AP
Anti-ACE2 (1/200)	R&D systems	Cat#AF933
Anti-TMPRSS2 (1/1000)	Thermo Fischer Scientific	Cat#MA5-35756
Anti-β-actin (1/10000)	Sigma-Aldrich	Cat#A2228
Anti-GAPDH (1/1000)	Sigma-Aldrich	Cat#MAB374
Anti-SARS-CoV-2 nucleocapsid (1/100)	Invitrogen	Cat#MA5-36271
Anti-ZO-1-Alexa Fluor-488 (1/100)	Invitrogen	Cat#339188
Goat anti-rabbit HRP (1/5000)	Cell Signalling Technology	Cat#7074
Horse anti-mouse HRP (1/5000)	Cell Signalling Technology	Cat#7076
Rabbit anti-Goat-HRP (1/10000)	Invitrogen	Cat#A27014
Goat anti-rabbit antibody-Alexa Fluor-633 (1/100)	Invitrogen	Cat#A21070
Bacterial and virus strains		
SARS-CoV-2, strain BetaCoV/France/IDF0571/2020	Pizzorno et al.[10]	accession ID EPI_ISL_411218
Chemicals, peptides, and recombinant proteins		
3,3′,5,5′-tetramethylbenzidine	Cell Signalling Technology	#7004
Boc-Gln-Ala-Arg-AMC	R&D Systems	Cat#ES014
Camostat mesylate	R&D Systems	Cat#3193
Critical commercial assays		

TruSeq Stranded mRNA kit	Illumina	Cat#20020595
KAPA Library quantification kit for Illumina Libraries	Kapa Biosystems	Cat#0796040001
Clarity™ Western ECL Substrate	Biorad	Cat#170-5061
Human Magnetic Luminex assay	R&D Systems	Custom Cat#LXSAHM-24
Human IL-8 ELISA	R&D Systems	Cat#DY208
Deposited data		
BCQ19	https://en.quebeccovidbiobank.ca	Release 11
RNAseq	https://www.ebi.ac.uk/biostudies/arrayexpress/	E-MTAB-14481
Computer code	https://github.com/GENOM-IC-Cochin/RNA-Seq_analysis	
Proteomics data	https://www.ebi.ac.uk/pride/	PXD055635
Experimental models: Primary cells		
Infection experiments		
Human Airway epithelial cells MucilAir™ Female, 56 years (y), Non-smoker, No pathology reported	Epithelix	MD078701
Human Airway epithelial cells MucilAir™ Male, 48y, Non-smoker, No Pathology reported	Epithelix	MD082201
Human Airway epithelial cells MucilAir™ Male, 27y, Non-smoker, No Pathology reported	Epithelix	MD080101

Human Airway epithelial cells MucilAir™ Female, 52y, Non-smoker, No Pathology reported	Epithelix	MD081001
Human Airway epithelial cells MucilAir™ Male, 27y, Non-smoker, CF, *CFTR* F508del homozygous	Epithelix	CF-MD43702
Human Airway epithelial cells MucilAir™ Female, 30y, Non-smoker, CF, *CFTR* F508del homozygous	Epithelix	CF-MD67901
Human Airway epithelial cells MucilAir™ Female, 33y, Non-smoker, CF, *CFTR* F508del homozygous	Epithelix	CF-MD051902
Human Airway epithelial cells MucilAir™ Male, 22y, Non-smoker, CF, *CFTR* F508del homozygous	Epithelix	CF-MD063701
Human Airway epithelial cells MucilAir™ Female, 31y, Smoker (<1 pack per day (PPD) x 17y), COPD	Epithelix	MD068301
Human Airway epithelial cells MucilAir™ Female, 53y, Smoker (3 PPD x 30 y), COPD	Epithelix	MD047201
Human Airway epithelial cells MucilAir™ Male, 58y, Smoker (1/2 PPD x 40 y), COPD	Epithelix	MD068901
Human Airway epithelial cells MucilAir™ Male, 60y, Smoker (1 PPD x 45 y), COPD	Epithelix	MD077701
TMPRSS2 activity		
Human Airway epithelial cells MucilAir™ Male, African American, 17y, No Smoker, No Pathology reported	Epithelix	MD0889
Human Airway epithelial cells MucilAir™ Female, African American, 54y, No smoker, No Pathology reported	Epithelix	MD0868
Human Airway epithelial cells MucilAir™ Female, 21y, No Smoker, CF, *CFTR* F508del homozygous	Epithelix	MD0607

Human Airway epithelial cells MucilAir™ Male, Caucasian, 58y, Smoker (2 PPD x 22 y), COPD	Epithelix	MD0903
Oligonucleotides		
Primers for nsp14: HKU-ORF1b-nsp14F: 5′-TGGGGYTTTACRGGTAACCT-3′; reverse primer HKU-ORF1b-nsp14R: 5′-AACRCGCTTAACAAAGCACTC-3′; probe HKU-ORF1b-nsp141P: 5′-FAM-TAGTTGTGATGCWATCATGACTAG-TAMRA-3′)	Eurogentech	
GAPDH Taqman® gene expression assay	Applied Biosystems	Hs02786624_g1
C3 Taqman® gene expression assay	Applied Biosystems	Hs00163811_m1
CFB Taqman® gene expression assay	Applied Biosystems	Hs00156060_m1
Software and algorithms		
AOZAN software	ENS Paris	
STAR algorithm	https://github.com/alexdobin/STAR/releases	Version 2.5.2b
Picard tools	https://github.com/broadinstitute/picard/releases/tag/3.2.0	Version 2.8.1
Featurecount	https://subread.sourceforge.net	Version Rsubread1.24.1

DESeq2 package	https://bioconductor.org/packages/release/bioc/html/DESeq2.html	Version 1.14.1
DIA-NN	https://github.com/vdemichev/DiaNN	Version 1.8.1
ProStaR software	https://www.bioconductor.org/packages/release/bioc/html/Prostar.html	Version 1.28.0
ShinyGO	http://bioinformatics.sdstate.edu/go/	Version 0.80
STRING	https://string-db.org	Version 12.0
Metascape	https://metascape.org/gp/index.html#/main/step1	Version 3.5.20240101
Jvenn	https://jvenn.toulouse.inrae.fr/app/example.html	
VolcaNoseR	https://huygens.science.uva.nl/VolcaNoseR/	
ClustVis	https://biit.cs.ut.ee/clustvis/	
ImageJ	https://imagej.net	
Prism 10.00	https://www.graphpad.com	

Biorender	https://www.biorender.com	
Other		
Column RP-C18 Aurora 2	IonOpticks	25 cm, 75 µm i.d., 120 Å, 1.6 µm